A Heuristic Model of Dansgaard–Oeschger Cycles. Part I: Description, Results, and Sensitivity Studies

HANSI A. SINGH

Department of Atmospheric Sciences, University of Washington, Seattle, Washington

DAVID S. BATTISTI

Department of Atmospheric Sciences, University of Washington, Seattle, Washington, and Geophysical Institute, University of Bergen, Bergen, Norway

CECILIA M. BITZ

Department of Atmospheric Sciences, University of Washington, Seattle, Washington

(Manuscript received 19 September 2012, in final form 2 October 2013)

ABSTRACT

A simple model for studying the Dansgaard–Oeschger (D-O) cycles of the last glacial period is presented, based on the T. Dokken et al. hypothesis for D-O cycles. The model is a column model representing the Nordic seas and is composed of ocean boxes stacked below a one-layer sea ice model with an energy-balance atmosphere; no changes in the large-scale ocean overturning circulation are invoked. Parameterizations are included for latent heat polynyas and sea ice export from the column. The resulting heuristic model was found to cycle between stadial and interstadial states at times scales similar to those seen in the proxy observational data, with the presence or absence of perennial sea ice in the Nordic seas being the defining characteristic for each of these states. The major discrepancy between the modeled oscillations and the proxy record is in the length of the interstadial phase, which is shorter than that observed. The modeled oscillations were found to be robust to parameter changes, including those related to the ocean heat flux convergence (OHFC) into the column. Production of polynya ice was found to be an essential ingredient for such sustained oscillatory behavior. A simple parameterization of natural variability in the OHFC enhances the robustness of the modeled oscillations. The authors conclude by discussing the implications of such a hypothesis for the state of the Nordic seas today and its state during the Last Glacial Maximum and contrasting the model to other hypotheses that invoke large-scale changes in the Atlantic meridional overturning circulation for explaining millennial-scale variability in the climate system. An extensive time-scale analysis will be presented in the future.

1. Introduction and motivation

a. Evidence for D-O cycles

Ice cores from Greenland [Greenland Ice Core Project (GRIP), North Greenland Ice Core Project (NGRIP), and Greenland Ice Sheet Project (GISP)] show that the high-latitude climate system experienced unusually large, abrupt warmings during the last ice age. These abrupt warmings are now known as Dansgaard–Oeschger (D-O) events, in honor of scientists W. Dansgaard and H. Oeschger (see, e.g., Dansgaard et al. 1993, 1984). The Greenland ice cores suggest that a typical D-O event is characterized by an abrupt warming of surface temperatures from glacial conditions (approximately −30°C) to near-interglacial conditions (approximately −20°C) over the Greenland ice sheet. This transition from glacial to interglacial conditions occurs rapidly, on a time scale of 20 yr or less. The ensuing period of interglacial conditions persists anywhere from 100 to 600 yr, over which time gradual surface cooling occurs. At the end of this interstadial phase, a more rapid decline in temperature harkens a return to glacial conditions. The sum of the

Corresponding author address: Hansi Singh, Department of Atmospheric Sciences, University of Washington, 408 Atmospheric Sciences-Geophysics (ATG) Building Box 351640, Seattle, WA 98195-1640.
E-mail: hansi@atmos.washington.edu

DOI: 10.1175/JCLI-D-12-00672.1

© 2014 American Meteorological Society

stadial and interstadial phases, corresponding to a full cycle period, appears to be on the order of 1500 yr, which we call a D-O cycle.

D-O cycles are evident in the ice cores and other records between 30 000 and 70 000 yr ago, and they are notably absent during the Last Glacial Maximum itself. Authors have, variously, reported anywhere between 20 and 27 D-O cycles, depending on the criteria for defining a D-O cycle (see Dansgaard et al. 1993; Rahmstorf 2002). From our current collection of proxy records of the geologic past, the D-O cycles constitute the most robust form of millennial-scale variability in the climate system. We point the reader to the recent review papers by Rahmstorf (2002), Alley (2007), and Clement and Peterson (2008) for evidence of the global signature of D-O cycles during the last glacial period.

Evidence for large-scale ocean circulation changes occurring in concert with D-O events is mixed. There is ample evidence for abrupt changes in the overturning circulation in the North Atlantic associated with the abrupt cooling events that occurred during the last deglaciation known as Heinrich 1 and the Younger Dryas [see the review by Alley (2007)], Arguably, only one published study provides convincing evidence that D-O events themselves are coordinated with changes in the ocean circulation. Keigwin and Boyle (1999) examined planktonic and benthic organisms at the Bermuda rise in the Atlantic and found that marked increases in sea surface temperature (SST) in the North Atlantic during marine isotope stage 3 [about 32–58 kyr before present (BP)] were concomitant with increases in deep-water formation and ventilation of the North Atlantic and that these changes plausibly align with the stadial to interstadial transitions in Greenland. In contrast, a review by Elliot et al. (2002) concluded there is little relationship between deep-water formation and D-O cycles in the northeast Atlantic, suggesting that large-scale ocean circulation changes are not coincident with the D-O events themselves.

In contrast to the mixed evidence for D-O-related changes in the North Atlantic Ocean, there is ample evidence for large changes in the hydrographic structure in the Nordic seas. For example, Rasmussen and Thomsen (2004) studied planktonic and benthic foraminifera from several sedimentary cores from the Nordic seas and found that significant differences in the local temperature and salinity profile accompanied the stadial and interstadial phases of the D-O cycles: high SSTs (5°–7°C) and cool deep waters (−0.5°C) at the start of the interstadial phase, decreasing SSTs and slightly warmer deep waters at the end of the interstadial, and ice-covered surface waters and warming deep waters (2°–8°C) during the stadial. Recent isotopic planktonic and benthic foraminiferal data published in Dokken et al. (2013) also link the stadial and interstadial phases of the D-O cycles to strong and weak brine production, respectively, suggesting differences in sea ice growth, both locally and offshore, during the stadial and interstadial phases. In both of these studies, the interstadial phase coincides with a hydrographic structure in the Nordic seas similar to that seen today; in contrast, the stadial phase coincides with one similar to that seen in the present-day Arctic Ocean.

b. *Proposed mechanisms*

One major hypothesis for D-O cycles invokes an instability in the Atlantic meridional overturning circulation (AMOC) in glacial times (despite the mixed proxy evidence for changes in the North Atlantic circulation, as described in section 1a). The AMOC hypothesis explains D-O cycles by a hysteresis in the state of the AMOC, wherein the meridional circulation abruptly switches between a warm state, where overturning is robust and sinking occurs at high latitudes, to a cold state, where overturning is weak and sinking occurs at midlatitudes. Weaver et al. (1991) and Winton and Sarachik (1993) found that it is possible to make the AMOC oscillate in an ocean-only model with steady, mixed surface boundary conditions.

Later work by de Verdière and Raa (2010) found that such oscillations were still a robust feature of an Earth system model of intermediate complexity (EMIC); they also found that the magnitude of the oscillations was damped by the sea ice response. A large increase in ocean heat transport to the high latitudes and a salinity-driven jump in the equator to pole density gradient are both features of the AMOC switch mechanism in this model. Furthermore, oscillations were found to exist only when a sufficiently large freshwater forcing was imposed; forcings lower than this threshold did not produce oscillations.

Along a similar vein, Loving and Vallis (2005) conducted a series of experiments with another EMIC and found that, when the atmospheric boundary was sufficiently cold, the AMOC spontaneously underwent millennial time-scale oscillations. Large shifts in the sea ice edge enhanced the magnitude of the oscillations and widened the regime over which they occurred. While the system was found to oscillate in the cold state (i.e., when the atmospheric emissivity was set appropriately low), surface freshening did not support oscillations: the key determinant of whether the meridional overturning would oscillate between weak and strong states was the temperature state of the atmosphere, not the surface salinity forcing. The reason for the different results obtained by Loving and Vallis (2005) and de Verdière and

Raa (2010) regarding the importance of sea ice for the millennial oscillations and the necessity for a strong salinity forcing are unclear.

Another class of hypotheses invokes some form of time-varying external forcing to cause the AMOC to switch between its warm and cold states: usually a periodic freshwater release from Northern Hemispheric ice sheets into the Atlantic Ocean (see Rahmstorf 2002, and references therein). While the behavior of ice sheets on millennial time scales is not well understood, modeling work on ice sheet binge–purge cycles (see, e.g., MacAyeal 1993) suggests one possible mechanism for such a periodic freshwater forcing. Although periodic freshwater forcing of the AMOC is the most widely accepted modus operandi of the D-O cycles, observational evidence for ice-rafted debris (IRD) accompanying each D-O cycle remains mixed. Bond and Lotti (1995) examined sediment cores in the North Atlantic and found that enhanced IRD is associated with the cold phase of the D-O cycles, albeit using only three tie points between the sediment core chronologies and the chronology of the Greenland record of the D-O cycles. Elliot et al. (2001) found that millennial-scale excursions in IRD were coordinated with magnetic susceptibility in sediment cores in the North Atlantic, with high IRD associated with cold conditions (low magnetic susceptibility) in the North Atlantic. On the other hand, Dokken and Jansen (1999) and Dokken et al. (2013) examined a high-sedimentation-rate core taken from the Nordic seas and concluded enhanced IRD was associated with the warm phase of the D-O cycle.

The modeling evidence for episodic freshwater forcing of the AMOC is also mixed. Most EMICs and global circulation models (GCMs) subject to freshwater forcing in the North Atlantic exhibit air temperature changes over Greenland that are less than half the magnitude of that seen in the proxy record (see, e.g., Okumura et al. 2009; Schmittner and Stocker 2001; Rahmstorf 2002; Vellinga and Wood 2002), with EMICs displaying significantly lower sensitivity to the hosing than GCMs (Stouffer et al. 2006). The only GCM simulations that record a strong, persistent response to freshwater forcing in the North Atlantic are those performed in a Last Glacial Maximum (LGM) configuration (Bitz et al. 2007; Otto-Bliesner and Brady 2010), suggesting that the sensitivity of the AMOC to freshwater input depends on the initial state of the climate system (Swingedouw et al. 2009). Most notably, Ganopolski and Rahmstorf (2001) find that a smooth, periodic forcing can give rise to D-O-like cycles in an EMIC, with abrupt warming similar in magnitude to that seen in the proxy record. In sum, observational and modeling evidence supporting the hypothesis that a periodic freshwater forcing of the AMOC could be responsible for the D-O cycles is promising but remains inconclusive.

Another hypothesis invoked for explaining the D-O cycles invokes excursions in the extent and thickness of sea ice in the high latitudes and the resulting shifts in position of the sea ice edge in the North Atlantic as the driving force for the D-O oscillations [for a review of such hypotheses, see Clement and Peterson (2008)]. Such hypotheses sometimes include secondary changes in the AMOC. Modeling studies show that changes in sea ice appear to be integral to D-O cycles. Li et al. (2005) showed that changes in wintertime sea ice extent in the Nordic seas can account for the changes in temperature and accumulation at Greenland like those seen in the proxy data. Chiang et al. (2003) and Chiang and Bitz (2005) showed that changes in sea ice extent also affect SSTs throughout the Northern Hemisphere and cause meridional displacement in the position of the intertropical convergence zone that could explain precipitation changes seen during a D-O cycle. Changes in sea ice extent in the Northern Hemisphere have also been linked to the position of the midlatitude jet, the strength of the Hadley cell, the position and intensity of the midlatitude storm tracks (Li and Battisti 2008), and changes in monsoonal precipitation patterns (Pausata et al. 2011).

The sea ice hypothesis, however, is not without drawbacks. The major issues are twofold: 1) as of yet, there are no proxy records that can be used to infer directly the thickness and extent of sea ice during the D-O cycles and 2) the exact mechanism by which sea ice changes on millennial time scales remains unknown.

c. The Dokken et al. hypothesis for D-O cycles

Motivated by a lack of clear proxy evidence for changes in the AMOC associated with D-O events, in this study we examine whether the D-O cycles can be understood as an intrinsic oscillation of the atmosphere–sea ice–ocean system that is local to the Nordic seas, as hypothesized by Dokken et al. (2013), and independent of large-scale changes in the overturning circulation. This idea stems from earlier laboratory and theoretical work by Welander and colleagues (see Welander 1977; Welander and Bauer 1977; Welander 1982), who showed that a tank of freshwater heated from below and cooled from above could exhibit self-sustaining overturning oscillations indefinitely. They theorized that the driving force for such oscillations is the competing effects related to how heat is transferred from the base of the fluid to the surface: heat transfer is efficient when the base is warm and the surface is cold until ice forms, and then surface heat loss is inhibited. Eventually, however, enough heat builds below to initiate convection, thereby

melting the ice. Later experimental work showed that such self-sustained relaxation oscillations are a robust feature of seawater that is heated from below and cooled from above. A tank of seawater will oscillate indefinitely with a periodicity that depends on the imposed heat fluxes, the vertical length scale of the tank, and the salinity of the seawater. In their experiments, a fresher, well-mixed layer in contact with ice lies above a saltier reservoir below. Heating of the bottom reservoirs results in eventual instability, and the entire water column overturns rapidly, resulting in abrupt loss of the sea ice. Eventually, however, persistent surface cooling allows ice to regrow, and the cycle continues ad infinitum. While such oscillations may be found to persist indefinitely in theoretical models and in laboratory studies, it has remained unclear what relevance such experiments have for the Earth's atmosphere–ocean–ice system.

We introduce a new hypothesis to describe the D-O cycles invoking the characteristics of atmosphere–sea ice–ocean oscillations as described by Welander and colleagues and the specific state of the regional climate (perennially ice covered, seasonally ice covered, or perennially ice free) within the Nordic seas during glacial times. In the ocean, our hypothesis invokes local hydrographic changes in the Nordic seas, as evidenced by regional paleo-proxy sedimentary data from Rasmussen and Thomsen (2004) and Dokken et al. (2013), changes that coincide with thermohaline oscillations within the region; however, no large-scale ocean circulation changes in the Atlantic are invoked.

Following Dokken et al. (2013), we propose that the precise etiology of the D-O cycles is as follows. During the stadial phase of the D-O cycles, the Nordic seas are covered in sea ice and conditions are relatively quiescent in the North Atlantic. The seasonal cycle of sea ice growth and melt is enough to enhance stratification in the upper ocean: brine rejection during sea ice growth enhances the cold halocline while sea ice melt serves to lighten the surface mixed layer. Vertical mixing below the halocline is merely diffusive. On the other hand, a small amount of ocean heat convergence below the pycnocline slowly raises the temperature of this deep region.

For a millennium or so, the water column remains stable. When the deep ocean warms enough to render the water column unstable, the entire water column overturns, bringing warm water into contact with the sea ice. As a consequence, the climate system transitions into the interstadial phase of the cycle.

During the interstadial phase, the Nordic seas are seasonally ice free. The stirring of the upper ocean by surface-level winds is vigorous. The water column is poorly stratified, and the cold halocline is nonexistent. The mixed layer is deep and warm, heated effectively by incoming solar radiation and by a persistent but small amount of ocean heat transport, which is now focused near the surface. This ice-free state, however, does not last: as turbulent surface fluxes cool the surface, sea ice reforms, the upper ocean begins to restratify, and the cold halocline begins to reemerge. On the other hand, the growth of sea ice also prevents the upper ocean from releasing stored heat, thereby slowing the stratification process and prolonging the onset of the stadial phase of the cycle. Eventually, the surface of the water column is cool enough for perennial sea ice cover to return to the Nordic seas, ending the interstadial phase.

Throughout the D-O cycle, we assume that the sinking branch of the AMOC terminates south of the Nordic seas, in agreement with long-equilibration GCM LGM simulations (Brandefelt and Otto-Bliesner 2009). As a consequence, only a small amount of heat is transported into the Nordic seas compared to the transport in the modern climate (less than 10%), and the heat transport is only weakly dependent on the phase of the D-O cycle.

This paper and one to follow will develop a numerical model of the D-O cycles based on the conceptual picture presented so far. The D-O cycles occurred over a large span of the last glacial period, which suggests that a D-O model must exhibit such cycling behavior over a substantial, physically relevant swath of the model's parameter space. An advantage of developing a simple, relatively tractable model is that the time scales involved in the D-O cycles can be analyzed and explained: why does each phase of the cycle have its own distinct time scale, and why are the transitions between the phases asymmetric? Such conundrums could be used to test the validity of the conceptual hypothesis and could provide a physical understanding of the D-O events themselves.

This paper will introduce the numerical model in detail, present the basic behavior of the model in a control parameter regime, and go on to describe the sensitivity of the model to key parameter values and to validate its robustness. An ensuing paper will focus on providing both mathematical expressions and conceptual explanations for the time scales seen in the models, including the length of the stadial and interstadial phases and the time scale over which transitions between the phases occur. Taken together, these studies will serve to introduce a new quantitative framework for understanding the D-O events.

2. Model description

a. Model overview, geometry, and state variables

Figure 1 provides an overview of the model geometry and the state variables associated with each component of the system. The model is columnar, representing the

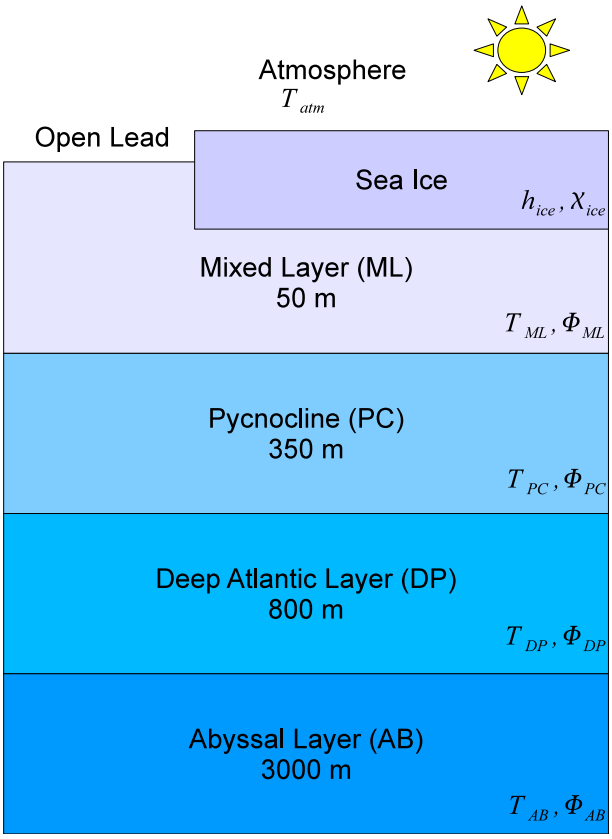

FIG. 1. Basic geometry of the model. The model is columnar and consists of four oceanic boxes (with default depths as labeled), sea ice, and a basic energy-balance atmosphere.

area-averaged Nordic seas, and consists of a simple seasonally varying energy-balance atmosphere overlying evolving sea ice and four stacked oceanic boxes. The surface atmospheric temperature T_{atm} is the principal state variable for the atmosphere and consists of two key components: a surface air temperature over sea ice $T_{\text{atm}}^{\text{seaIce}}$ and a surface air temperature over open water $T_{\text{atm}}^{\text{lead}}$. The sea ice model has associated state variables for the thickness of the sea ice h_{ice} and the fraction of the column covered by sea ice χ_{ice}. The ocean consists of four boxes. The state variables associated with the ith ocean box are its temperature T_i and salt content Φ_i. All boxes have constant depths with default values set similarly to the present-day vertical distribution of temperature and salinity in the Arctic [as described by Aagaard et al. (1981)]: a mixed layer (ML) of 50-m depth, a pycnocline layer (PC) of 300-m depth, a deep layer (DP) of 800-m depth, and an abyssal layer (AB) of 3000-m depth.

When developing this heuristic column model, we have made the following major assumptions:

- Positive or negative energy imbalances at the top and bottom faces of the sea ice drive ice melt or growth, respectively. In other words, we assume that the sea ice has zero heat capacity (see Semtner 1976).
- We assume that the brine rejected from growing sea ice interleaves within the PC box rather than the ML box (as in Duffy et al. 1999; Nguyen et al. 2009). On the other hand, we assume that sea ice melt freshens the ML box. In this way, sea ice growth and melt acts as a salt pump and drives ocean stratification.
- The amount of sea ice in the column plays a role in determining the amount and distribution of OHFC (Aagaard et al. 1981). An ice-free column will converge heat within surface layers, while an ice-covered column will converge smaller amounts of heat at depth.
- The amount of sea ice in the column governs the strength of wind-driven mixing between the surface layers (Kraus and Turner 1967).
- We parameterize sea ice production in polynyas and sea ice export processes. Additional sea ice (and its attendant brine) is imported into the column from offshore polynyas, while winds and currents export ice from the column into the North Atlantic.
- We assume that, during the last glacial period, precipitation and runoff into the Nordic seas are negligible. The former point is consistent with GCM simulations, which display topographical steering of the jet and the midlatitude storm track by the Laurentide ice sheet such that they are positioned well to the south of the Nordic seas (as in Li and Battisti 2008; Braconnot et al. 2007; Laînè et al. 2009). As a consequence, advective salt fluxes into the upper ocean layers (which would be expected to balance such surface freshwater fluxes) are also assumed to be negligible.
- As seen in GCM simulations of the last glacial period, we assume that the AMOC is shifted south of the Nordic seas (see Li and Battisti 2008; Brandefelt and Otto-Bliesner 2009). Thus, the AMOC has little influence on conditions in the Nordic seas during the both the stadial and interstadial phases of the D-O cycles.
- Over millennial time scales, the column is salt conserving. This allows the model to be integrated for thousands of years.

Figure 2 provides an overview of the different salt and heat fluxes or flux convergences (designated with Q and W, respectively) that determine the temperature and salinity evolution of the model components.

b. *Ocean box temperature evolution*

In general, the temperature evolution of each ocean box may be described by the ordinary differential equation (ODE),

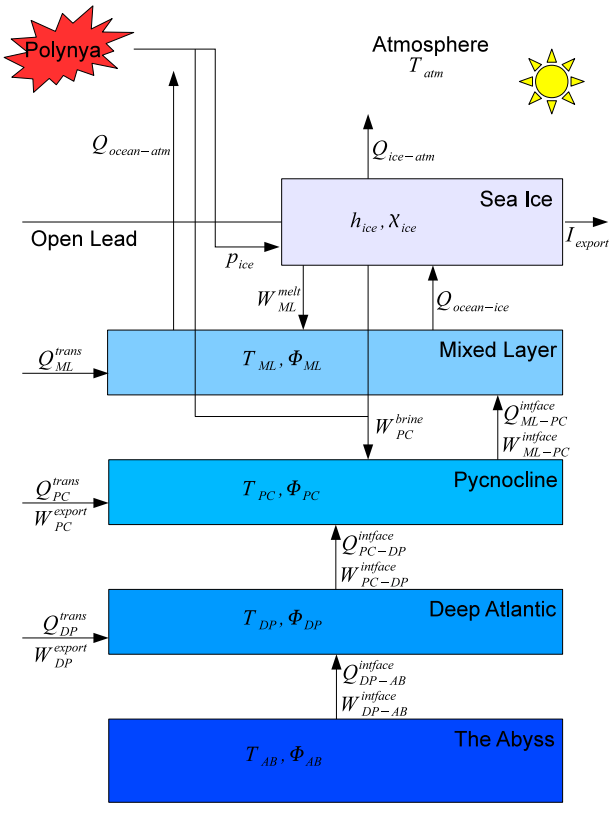

FIG. 2. In-depth geometry of the model, with surface and interfacial fluxes labeled. The state variables for the ocean boxes are T_i and Φ_i, while the state variables for the sea ice are h_{ice} and χ_{ice}. Heat fluxes are represented by Q_i, and salt fluxes are described by W_i. Ice source and sink terms (from polynyas and ice export, respectively) are represented by p_{ice} and I_{export}, respectively.

$$m_i c_w \frac{dT_i}{dt} = Q_i^{\text{trans}} + Q_{i,i-1}^{\text{intface}} - Q_{i+1,i}^{\text{intface}}, \tag{1}$$

where T_i is the temperature of the layer, m_i is the mass of the layer, c_w is the specific heat capacity of water, Q_i^{trans} is the net ocean heat flux convergence (OHFC) into the box, and $Q_{i,i-1}^{\text{intface}}$ and $Q_{i+1,i}^{\text{intface}}$ are the interfacial eddy diffusive heat flux from the box below and above. We describe the OHFC parameterization in the following subsection and the interfacial flux formulation in section 2e.

We apply Eq. (1) to each ocean box as follows: The AB layer is relatively isolated, lying below the level of the Greenland–Scotland ridge. Therefore, we posit that there is negligible OHFC directly into the AB layer and only one interfacial flux, that from the DP box that lies directly above it: $Q_{\text{AB-DP}}^{\text{intface}}$. In contrast, the temperature of the DP box evolves as a result of both interfacial eddy diffusive heat fluxes from the boxes directly above ($Q_{\text{DP-PC}}^{\text{intface}}$) and below ($Q_{\text{AB-DP}}^{\text{intface}}$) and from OHFC into the layer $Q_{\text{DP}}^{\text{trans}}$. The temperature of the pycnocline evolves similarly to the DP box, driven by an OHFC $Q_{\text{PC}}^{\text{trans}}$ and interfacial fluxes from neighboring boxes above and below $Q_{\text{PC-ML}}^{\text{intface}}$ and $Q_{\text{DP-PC}}^{\text{intface}}$.

The mixed layer interacts with the atmosphere, sea ice, and pycnocline box, exchanging heat and salt. Consequently, the temperature of the ML evolves in a more complex manner than that of the other ocean boxes. The following equation for evolution of the ML follows that outlined by Thorndike (1992) but allows for fractional (incomplete) sea ice cover. In general, we posit that the temperature of the ML changes according to

$$m_{\text{ML}} c_w \frac{dT_{\text{ML}}}{dt} = (1-\chi_{\text{ice}})(Q_{\text{SW}}^{\text{net}} - Q_{\text{LW}}^{\text{net}} - Q_{\text{turb}}^{\uparrow}) - \chi_{\text{ice}} Q_{\text{ML-ice}} + Q_{\text{ML}}^{\text{trans}} + Q_{\text{PC-ML}}^{\text{intface}}. \tag{2}$$

In Eq. (2), $Q_{\text{ML}}^{\text{trans}}$ is the OHFC into the ML, $Q_{\text{SW}}^{\text{net}}$ is the net incoming shortwave solar radiation absorbed by the ML, $Q_{\text{LW}}^{\text{net}}$ is the net outgoing longwave radiation emitted by the ML, $Q_{\text{ML-ice}}$ is the heat flux between the ML and sea ice, and $Q_{\text{turb}}^{\uparrow}$ is the turbulent heat flux from the ML into the atmosphere. The surface fluxes (shortwave, longwave, and turbulent fluxes) are all described in section 2f. The heat flux between the ML and the overlying sea ice (when sea ice is present) is formulated using

$$Q_{\text{ML-ice}} = C_0 (T_{\text{ML}} - T_{\text{ice}}^{\text{bottom}}), \tag{3}$$

where $C_0 = 20\,\text{W m}^{-2}\,^{\circ}\text{C}^{-1}$ and $T_{\text{ice}}^{\text{bottom}} = -1.8^{\circ}\text{C}$.

OHFC FORMULATION

We formulate the OHFC in a manner consistent with our hypothesis: namely, that the sinking branch of the AMOC is shifted south of the Nordic seas during the glacial period and is relatively impervious to changes in sea ice and hydrography therein. As a result, the OHFC into the Nordic seas is reckoned to be a fraction of that seen in the modern climate: on the order of $1\,\text{W m}^{-2}$, rather than the $35\,\text{W m}^{-2}$ converging into the region today (Hansen and Osterhus 2000). In fact, the OHFC values we use in our model are comparable to that seen in the present-day Arctic (Aagaard et al. 1981). Furthermore, we distribute this heat between the ocean layers in a manner that is dependent on the sea ice cover: into the top layers of the ocean (the ML and PC boxes) when the sea ice cover is thin and seasonal and into the deep ocean (the DP box) when the sea ice cover is substantial and the surface ocean is well stratified. The latter point is consistent with the OHFC into the Arctic as described by Aagaard et al. (1981), who showed that

TABLE 1. Values of Q_X^{trans}, the OHFC, into the model ocean boxes. Both the general formulation and the specific formulation (during ice-covered and ice-free conditions) are shown.

Ocean box	General	$\chi_{\text{ice}} = 1$ (ice present)	$\chi_{\text{ice}} = 0$ (ice free)
ML: $Q_{\text{ML}}^{\text{trans}}$	$^2/_3 Q_{\text{tot}}^{\text{NoIce}}(1-\chi_{\text{ice}})$	0	$2.0\,\text{W m}^{-2}$
PC: $Q_{\text{PC}}^{\text{trans}}$	$^1/_3 Q_{\text{tot}}^{\text{NoIce}}(1-\chi_{\text{ice}})$	0	$1.0\,\text{W m}^{-2}$
DP: $Q_{\text{DP}}^{\text{trans}}$	$Q_{\text{tot}}^{\text{Ice}}\chi_{\text{ice}}$	$0.5\,\text{W m}^{-2}$	0
AB	0	0	0
Total	Sum of above	$Q_{\text{tot}}^{\text{Ice}} = 0.5\,\text{W m}^{-2}$	$Q_{\text{tot}}^{\text{NoIce}} = 3.0\,\text{W m}^{-2}$

warm, salty water transported from the Atlantic into the Arctic will subduct beneath a cold halocline (as posited to exist in the Nordic seas during stadial conditions, when sea ice cover is perpetual) and enter the water column at great depth (>500 m).

Table 1 describes the notation for and typical values of the OHFC into the model ocean boxes. The vertical distribution of OHFC depends strongly on χ_{ice}, the sea ice fraction in the column, while the magnitude of the OHFC depends only mildly on this quantity. In particular, we parameterize the OHFC into the DP layer as $Q_{\text{DP}}^{\text{trans}} = \chi_{\text{ice}} Q_{\text{tot}}^{\text{Ice}}$, where $Q_{\text{tot}}^{\text{Ice}} = 0.5\,\text{W m}^{-2}$ and χ_{ice} is the sea ice fraction. For the PC layer,

$$Q_{\text{PC}}^{\text{trans}} = (1-\chi_{\text{ice}})\frac{1}{3}Q_{\text{tot}}^{\text{NoIce}}, \tag{4}$$

where $Q_{\text{tot}}^{\text{NoIce}}$ is the total OHFC when the system is in an ice-free state, reckoned to be $3\,\text{W m}^{-2}$ in the control simulation. Analogous to the PC, the OHFC into the ML is nil when the column is ice covered but is nonzero when the column is ice free,

$$Q_{\text{ML}}^{\text{trans}} = (1-\chi_{\text{ice}})\frac{2}{3}Q_{\text{tot}}^{\text{NoIce}}. \tag{5}$$

In Eqs. (4) and (5), the factors of $^1/_3$ and $^2/_3$ permit us to partition the OHFC between the PC and ML boxes, respectively, allowing for the heating to be surface weighted such that a greater fraction converges in the ML box than in the PC box.

c. Sea ice evolution

We model the seasonal growth and melt of the sea ice after Thorndike (1992). When sea ice cover is complete (there is no open water), the sea ice evolves according to

$$\rho_{\text{ice}} L_f \frac{dV_{\text{ice}}}{dt} = -Q_{\text{ML-ice}} + Q_{\text{LW}}^{\text{net}} - Q_{\text{SW}}^{\text{net}} + \rho_{\text{ice}} L_f \frac{dp_{\text{ice}}}{dt} - I_{\text{export}}, \tag{6}$$

where ρ_{ice} is the density of sea ice, L_f is the heat of fusion for seawater, V_{ice} is the volume of the ice, $Q_{\text{ML-ice}}$ is the heat flux into the ice from the ML [formulated according to Eq. (3)], $Q_{\text{SW}}^{\text{net}}$ is the net shortwave radiation incident on the ice, $Q_{\text{LW}}^{\text{net}}$ is the net longwave radiation at the top surface of the ice, dp_{ice}/dt is a sea ice source term to model distally formed sea ice advected into the column from polynyas, and I_{export} is a sea ice sink term to model ice export from the Nordic seas. The formulation of the shortwave, longwave, and atmospheric heat transport fluxes in Eq. (6) will be described in section 2f. We describe the polynya source and ice export sink terms in the following two paragraphs.

As described in Martin et al. (1998) and Cavalieri and Martin (1994), we posit that latent heat polynyas driven by katabatic winds blowing off the Fennoscandian ice sheet (FSIS) were responsible for the production of sea ice along the FSIS during the last glacial. This ice is then swept into the wider Nordic seas by winds and currents, accelerating ice growth beyond that expected from local conditions. In our model, we set $\int (dp_{\text{ice}}/dt)\,dt = 1.0$ m per cold season, provided that the sea ice thickness within the column is greater than or equal to 1.0 m. When h_{ice} is less than 1.0 m, there is no extra polynya ice added to the column. Note that brine rejected from polynya ice is also assumed to interleave into the PC layer, just like brine rejected from sea ice formed in situ.

We hypothesize that some of the sea ice formed within the Nordic seas during the last glacial cycle was exported from the Nordic seas into the North Atlantic. To account for the export of sea ice from the column, we formulate a yearly cumulative export term I_{export} as the integrated sum of the ice grown within the column per year, multiplied by an ice export factor C_r,

$$I_{\text{export}} = C_r \int_{1\text{yr}} \left(\frac{dV_{\text{ice}}^{\text{growth}}}{dt} \right) dt. \tag{7}$$

Each year, we remove a quantity of ice from the column I_{export}, which corresponds to the yearly export of $(100C_r)\%$ of the ice formed within the column per annum. We use $C_r = 0.05$, corresponding to the export of 5.0% of the ice formed within the Nordic seas per year.

When sea ice cover is incomplete and open water is present, energy conservation requires that the sea ice evolve according to

$$\rho_{\text{ice}} L_f \frac{dV_{\text{ice}}}{dt} = \chi_{\text{ice}}(Q_{\text{LW}}^{\text{net}} - Q_{\text{SW}}^{\text{net}} - Q_{\text{ML-ice}}) + \rho_{\text{ice}} L_f \frac{dp_{\text{ice}}}{dt} - I_{\text{export}}, \quad (8)$$

where χ_{ice} is the fraction of the column covered by sea ice. In general, the volume of sea ice present is related to the ice thickness h_{ice} and ice area by $V_{\text{ice}} = h_{\text{ice}}\chi_{\text{ice}}$. The ice fraction χ_{ice} may be diagnosed for a given h_{ice} using the following formulation:

$$\chi_{\text{ice}} = \begin{cases} 0 & \text{for} \quad h_{\text{ice}} = 0\,\text{m} \\ 2h_{\text{ice}} & \text{for} \quad h_{\text{ice}} \in (0, 0.5]\,\text{m} \\ 1 & \text{for} \quad h_{\text{ice}} > 0.5\,\text{m} \end{cases}. \quad (9)$$

Equation (8) reduces to Eq. (6) when $h_{\text{ice}} > 0.5\,\text{m}$, meaning that $\chi_{\text{ice}} = 1$.

d. Ocean salinity

We formulate the salinity evolution of the different components of the system using an equation for salt content (in units of grams salt) within the ith layer,

$$\frac{d\Phi_i}{dt} = W_{i,i-1}^{\text{intface}} - W_{i+1,i}^{\text{intface}} + W_i^x, \quad (10)$$

where $W_{i,i-1}^{\text{intface}}$ and $W_{i+1,i}^{\text{intface}}$ refer to the interfacial salt fluxes with layers below and above and W_i^x is a term representing horizontal or vertical advective fluxes of salt due to sea ice growth and melt, as well as transport processes (which we will detail further below). The salinity may be derived from the salt content using $S_i = \Phi_i/(\rho_i h_i)$, where h_i is the depth of the ith layer and ρ_i is its density. We compute the density of the box in this and all subsequent calculations using the full equation of state for seawater (from Gill 1982).

The salt content of the ML evolves due an interfacial salt flux from the PC $W_{\text{ML-PC}}^{\text{intface}}$ and a negative salt flux from sea ice melt $W_{\text{ML}}^{\text{melt}}$. Given a particular rate of sea ice melt dV_{ice}/dt and assuming (for simplicity) that sea ice has no salt content, the meltwater flux may be formulated as

$$W_{\text{ML}}^{\text{melt}} = \rho_{\text{ice}} \frac{S_{\text{ML}}^0}{\left(1 - \frac{S_{\text{ML}}^0}{1000}\right)} \frac{dV_{\text{ice}}^{\text{melt}}}{dt}, \quad (11)$$

where S_{ML}^0 is a reference salinity (taken to be the initial salinity of the mixed layer). We derive Eq. (11) from the assumption that the mass of ice melted per unit time results in a mass flux of salt-free water (equal to the mass flux of the melted ice) added to the mixed layer, thereby lowering its total salt content. Note that we use the reference salinity S_{ML}^0 to estimate the negative mass flux of salt associated with this sea ice melt rate. This allows the column to be salt conserving over time scales exceeding 1 yr, since the negative salt flux associated with sea ice melt is balanced by a positive salt flux into the pycnocline because of brine rejected when the sea ice was formed.

The salt content of the PC evolves because of brine rejected as a result of sea ice formation $W_{\text{PC}}^{\text{brine}}$; a freshwater recirculation flux resulting from ice export $W_{\text{PC,DP}}^{\text{export}}$ (see the following paragraph for a description of this term); and interfacial fluxes from the neighboring ML and DP boxes $W_{\text{ML-PC}}^{\text{intface}}$ and $W_{\text{PC-DP}}^{\text{intface}}$, respectively. As described in coupled modeling studies by Duffy et al. (1999) and Nguyen et al. (2009), we formulate our model so that all the brine rejected from sea ice formation (both within the column and in polynyas) is assumed to sink to the depth of the pycnocline and interleave therein, thereby enhancing the cold halocline. We formulate this salt flux into the pycnocline analogously to the negative salt flux into the ML resulting from sea ice melt, Eq. (11),

$$W_{\text{PC}}^{\text{brine}} = \rho_{\text{ice}} \frac{S_{\text{ML}}^0}{\left(1 - \frac{S_{\text{ML}}^0}{1000}\right)} \frac{dV_{\text{ice}}^{\text{grow}}}{dt}. \quad (12)$$

The salt content of the DP box evolves via interfacial fluxes from the neighboring boxes PC and AB boxes ($W_{\text{PC-DP}}^{\text{intface}}$ and $W_{\text{DP-AB}}^{\text{intface}}$, respectively), as well as a negative salt flux arising from ice export from the column $W_{\text{PC,DP}}^{\text{export}}$. We model this ice export term as follows:

$$\int_{1\text{yr}} W_{\text{PC,DP}}^{\text{export}}\, dt = \rho_{\text{ice}} \frac{S_{\text{ML}}^0}{\left(1 - \frac{S_{\text{ML}}^0}{1000}\right)} I_{\text{export}}. \quad (13)$$

The rationale behind this term is that ice exported from the Nordic seas into the North Atlantic, where it melts and is entrained into the sinking branch of the AMOC south of the Nordic seas, creating fresher water below that subsequently recirculates back into the Nordic seas at the level of the PC and DP layers. The ice export sink term causes the column to salinize over long time scales; including this freshening term allows the column to be salt conserving. The fraction of the negative salt flux added to the PC and DP is F_{PC} and $1 - F_{\text{PC}}$, respectively, where the default value of F_{PC} is taken to be 0.8. Finally,

the AB box evolves solely through an interfacial diffusive salt flux with the DP box $W^{\text{intface}}_{\text{DP-AB}}$.

e. Formulation of interfacial fluxes and convective mixing

We parameterize vertical mixing processes between ocean boxes as follows: When the system is stably stratified, the density of the underlying box j is greater than that of the overlying box i: $\rho_j > \rho_i$. In this case, mixing between boxes will be either eddy driven or diffusive, depending on the depth of the boxes involved. In general, interfacial mixing between the ith and jth box results in the following heat and salt fluxes:

$$Q^{\text{intface}}_{i,j} = \frac{2K^T_{i,j}c_w(\rho_i T_i - \rho_j T_j)}{h_i + h_j} \quad \text{and} \tag{14}$$

$$W^{\text{intface}}_{i,j} = \frac{2K^S_{i,j}(\rho_i S_i - \rho_j S_j)}{h_i + h_j}, \tag{15}$$

where h_i is the depth of the ith box and $K^X_{i,j}$ is the mixing coefficient for property X across the interface between boxes i and j. The assumption behind this formulation is that mixing across interfaces results in the exchange of equal volumes of seawater between boxes: water that carries the temperature and salinity properties of its parent box into its new residence, thereby changing the state variables of both boxes.

We have assigned the coefficients of vertical mixing $K^T_{i,j}$ and $K^S_{i,j}$ between each set of boxes based on the depth of the layers in question. As described in Wunsch and Ferrari (2004) and Gargett (1984), turbulent eddies are the dominant mode of vertical mixing within the top 200 m of the ocean. Such eddies mix heat and salt in the upper ocean, with the magnitude of the mixing coefficient on the order of $1 \times 10^{-4}\,\text{m}^2\,\text{s}^{-1}$ (as in Gargett 1984). In such a case, we expect that $K^T = K^S$, since both properties will be transported equally by eddy-driven mixing processes. We posit mixing at the interface between the ML and PC boxes is eddy driven, so $K^T_{\text{ML-PC}} = K^S_{\text{ML-PC}} = O(10^{-4})\,\text{m}^2\,\text{s}^{-1}$.

As described in Kraus and Turner (1967), the extent of mixing in the upper layer of the ocean is wind driven and therefore moderated by the fraction of ocean surface covered with sea ice. Therefore, we assign specific values to $K^{T,S}_{\text{ML-PC}}$ based on the extent of sea ice cover, as follows:

$$K^{T,S}_{\text{ML-PC}} = \chi_{\text{ice}} K^{T,S-\text{Ice}}_{\text{ML-PC}} + (1 - \chi_{\text{ice}}) K^{T,S-\text{NoIce}}_{\text{ML-PC}}. \tag{16}$$

In Eq. (16), we have assigned $K^{T,S-\text{Ice}}_{\text{ML-PC}} = 1 \times 10^{-4}\,\text{m}^2\,\text{s}^{-1}$ and $K^{T,S-\text{NoIce}}_{\text{ML-PC}} = 6 \times 10^{-4}\,\text{m}^2\,\text{s}^{-1}$. Equation (16) posits a larger amount of upper-ocean mixing when $\chi_{\text{ice}} < 1$ and a smaller amount of upper-ocean mixing when $\chi_{\text{ice}} \approx 1$.

On the other hand, vertical mixing at depths greater than 400 m is dominated by diffusive processes, as described by Huppert and Turner (1981). In this realm, heat and salt diffuse at separate rates, based on their molecular diffusivity. At a given depth, the molecular diffusivity of heat exceeds the molecular diffusivity of salt by a factor of at least 10, giving $K^T = 10K^S$. Furthermore, we expect that the magnitude of mixing between the PC and DP boxes is larger than that between the DP and AB boxes, because of the greater depth of the latter. Therefore, we have set the remainder of the vertical eddy diffusive coefficients as follows: $K^T_{\text{PC-DP}} = 10^{-5}\,\text{m}^2\,\text{s}^{-1}$, $K^S_{\text{PC-DP}} = 10^{-6}\,\text{m}^2\,\text{s}^{-1}$, $K^T_{\text{DP-AB}} = 10^{-7}\,\text{m}^2\,\text{s}^{-1}$, and $K^S_{\text{DP-AB}} = 10^{-8}\,\text{m}^2\,\text{s}^{-1}$.

When the density of an overlying box exceeds that of an underlying box, we assume mixing is done by convection. In this case, we completely mix the temperature and salinity in the two layers.

f. Formulation of surface conditions, processes, and fluxes

We diagnose the surface air temperature as an average of the surface temperature over open water T_{ML} and the surface air temperature over sea ice $T^{\text{top}}_{\text{ice}}$ weighted by the fraction of sea ice cover in the column,

$$T_{\text{atm}} = \chi_{\text{ice}} T^{\text{top}}_{\text{ice}} + (1 - \chi_{\text{ice}}) T_{\text{ML}}. \tag{17}$$

We describe the calculation of $T^{\text{top}}_{\text{ice}}$, the temperature at the top of the ice, in Eq. (22).

We formulate the surface processes included in Eq. (2), the equation governing the evolution of the ML box, and Eq. (6), the equation governing the evolution of the sea ice, as follows: First, following Thorndike (1992) we assign the mean shortwave flux reaching the surface during the warm half of the year as $F_{\text{SW}} \approx 200\,\text{W}\,\text{m}^{-2}$ and as $0\,\text{W}\,\text{m}^{-2}$ during the cold half. Taking into account the albedo α_i of the surface receiving the radiation, we obtain the following formulation for the net shortwave fluxes:

$$Q^{\text{net}}_{\text{SW}} = \begin{cases} (1 - \alpha_{\text{ice}})F_{\text{SW}} & \text{over sea ice in summer} \\ (1 - \alpha_{\text{ocn}})F_{\text{SW}} & \text{over open ocean in summer} \\ 0 & \text{over sea ice or open ocean in winter} \end{cases}. \tag{18}$$

Since $\alpha_{ice} \approx 0.6$ and $\alpha_{ocn} \approx 0.1$, the net shortwave flux absorbed during the warm half of the year by the ML and sea ice are 180 and 80 W m^{-2}, respectively.

Next, the net longwave flux in Eqs. (2) and (6) can be approximated as per Thorndike (1992) as follows:

$$Q_{LW}^{net} \approx \frac{A + BT_{surf}}{n} - D/2, \tag{19}$$

assuming the surface temperature (ocean mixed layer, sea ice, or both) is in equilibrium with the overlying atmosphere, where T_{surf} is the temperature of the surface; the constants A and B are equal to 320 W m^{-2} and 4.6 W m^{-2} °C^{-1}, respectively; and D, the atmospheric heat transport flux convergence, is taken to be 90 W m^{-2}. The quantity n refers to the optical depth of the atmosphere and may be used to approximate the effects of reabsorption and reemission between the surface and atmosphere. As in Thorndike (1992), n depends on season and sea ice cover. Thus, Eq. (19) becomes

$$Q_{LW}^{net} = \begin{cases} (A + BT_{ML})/n_s - D/2 & \text{over open ocean, summer} \\ (A + BT_{ML})/n_w - D/2 & \text{over open ocean, winter} \\ A/n_s - D/2 & \text{over sea ice, summer} \\ (A + BT_{ice}^{top})/n_w - D/2 & \text{over sea ice, winter} \end{cases}, \tag{20}$$

where $n_w = 2.5$ during the cold half of the year for both ice-covered and ice-free periods, $n_s = 2.8$ during the warm half of the year during ice-covered periods, and $n_s = 2.9$ during the warm half of the year during ice-free periods. During the warm half of the year, we assume $T_{ice}^{top} = 0$°C.

The temperature at the top of the ice during the cold half of the year is found from equating the energy fluxes at the top surface of the ice $Q_{LW}^{net} = Q_{cond}^{\uparrow}$, where $Q_{cond}^{\uparrow}$ is the conductive heat flux through the ice. From Thorndike (1992),

$$Q_{cond}^{\uparrow} = \frac{k(T_{ice}^{top} - T_{ice}^{bot})}{h_{ice}}. \tag{21}$$

Substituting Eqs. (21) and (20) into $Q_{LW}^{net} = Q_{cond}^{\uparrow}$ and solving for T_{ice}^{top} during the cold half of the year gives

$$T_{ice}^{top} = \frac{1}{B/n_{winter} + k/h_{ice}} \left(\frac{kT_{ice}^{bot}}{h_{ice}} - \frac{A}{n_{winter}} + \frac{D}{2} \right). \tag{22}$$

Finally, we approximate the atmosphere to ocean turbulent heat flux $Q_{turb}^{\uparrow}$ using a bulk formulation (as in Peixoto and Oort 1992), $Q_{turb}^{\uparrow} = B_T(T_{ML} - T_{ref})$, where $B_T \approx 5.0$ W m^{-2} °C^{-1} and T_{ref} is the minimum temperature the ML box may attain (−1.8°C).

g. Numerical methods

We used the forward Euler method to discretize the time derivatives found in the model equations. We integrated the model asynchronously in order to accommodate the very different time scales involved in the components. Surface processes, including those involving the atmosphere, mixed layer, and sea ice, evolve rapidly on scales shorter than a season (as described in Thorndike 1992). For these components, we used a time step of $\Delta t = 1/200$ yr. Middle and deep oceanic processes, however, have much slower time scales (Wunsch and Ferrari 2004), allowing integration of these components with a time step of $\Delta t = 1/20$ yr.

3. Model results

The model, as detailed in previous sections, replicates many of the essential features of the D-O cycles (see Fig. 3 for a 6000-yr integration of the standard model). We begin by considering the stadial phase in the standard model output, which is approximately 1100 yr long with perennial sea ice cover in the Nordic seas. Seasonally, the sea ice has a maximal thickness of approximately 3.0 m at the end of winter and a minimum thickness of 2.3 m at the end of summer (Fig. 4). With this perennial sea ice, surface air temperature is approximately −22°C during the cold season, for an average annual temperature of −11°C (Fig. 5). The temperatures in the upper-ocean boxes are also close to the freezing point, $T_{ML} \approx -2$°C and $T_{PC} \approx -1$°C. The temperature in the PC box, however, increases slightly over the course of the stadial period because of diffusive heat fluxes between the PC and DP boxes (not shown). The temperature in the DP box rises substantially, increasing from approximately 4.4° to 4.9°C over the 1100 yr of the stadial period (Fig. 6). Though the temperatures of the ML and PC are close throughout the stadial phase, their salinities are very different (Fig. 7). During the stadial, S_{PC} increases from 34.2 to 34.9 psu, while S_{ML} increases from 33.5 to 34.0 psu (Fig. 7), resulting in extremely strong density stratification in the upper ocean throughout this period (Fig. 8). Such a stable cold halocline is similar to that seen today in the Arctic Ocean under its perennial sea ice cover (Aagaard et al. 1981).

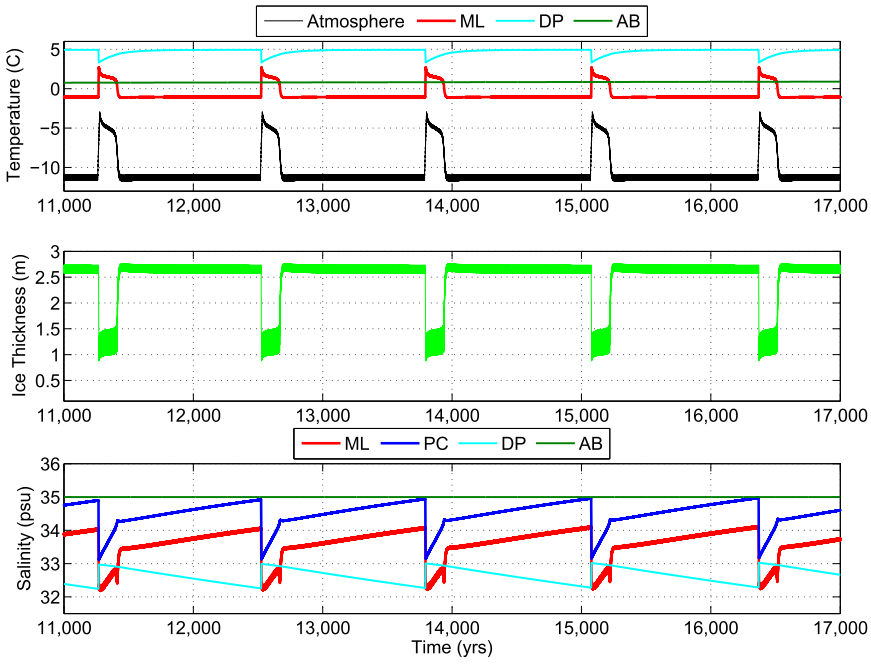

FIG. 3. Results for (top) atmosphere and ocean temperature, (middle) sea ice thickness, and (bottom) ocean salinity from 6000 yr of output from the model with default parameter values. Except for the atmospheric temperature, the model output, which reports all state variables biannually (once at the end of the warm season and again at the end of the cold season), has been smoothed with a 5-yr running-mean filter; the atmospheric temperature has been smoothed with a 25-yr running-mean filter to mirror the resolution of the δ^{18}O ice core proxy used to infer Greenland surface temperature. In (top), the temperature of the PC box is not shown; at the scale of this figure, the temperatures of the ML and PC are indistinguishable.

Finally, the salinity of the DP decreases slowly, from 32.8 to 32.2 psu, over the course of the stadial period (Fig. 7) because of sea ice exported into the Atlantic: sea ice export causes freshening of the Atlantic water that circulates in this layer (as diffusive exchange with the PC box would increase salinity and exchange with the AB box is negligible). Indeed, making the export coefficient C_r zero results in little net freshening of the DP layer (not shown).

The transition from the stadial to interstadial period is extremely rapid (as seen in Figs. 6 and 7), occurring over a brief 3-yr span (not shown). Convective overturning of the PC and DP boxes initiates the transition to the interstadial period. This overturning event is caused by a combination of factors, which all conspire to decrease ρ_{DP} and increase ρ_{PC}, thereby equalizing their densities and initiating convection (Figs. 8 and 9): the increase in the temperature of the DP layer (due to weak OHFC into the DP box), the decrease in the salinity of the DP layer, and the increase in the salinity of the PC layer (due to brine rejection from sea ice formation and subsequent export). The overturning of the PC and DP boxes quickly raises the temperature of the PC box to about 3°C at the start of the interstadial (Fig. 5). Next, the large temperature gradient between the ML and PC drives an upward flux of heat into the ML box through eddy-driven vertical mixing, thereby increasing the temperature of the mixed layer, increasing the ice–ocean conductive heat flux by several orders of magnitude, and allowing the perennial sea ice cover to melt rapidly, giving way to seasonal sea ice (Figs. 4 and 5). The overturning event also causes the salinities of the PC and DP boxes to equalize. The salinity of the mixed layer decreases rapidly because of abrupt sea ice melt during the stadial to interstadial transition, hitting a low point of $S_{ML} \approx 31.8$ psu (Fig. 4).

The interstadial phase is approximately 150 yr in length. The model output, particularly from Figs. 4 and 5, suggests that the interstadial period has several different phases. The first phase corresponds to the rapid decay of the PC box temperature from its maximum value of 3°C to about 2°C, a process that takes approximately 20 yr. After an initial adjustment process (<5 yr) in which the temperature of the ML box increases from −1.8° to 3°C (annually averaged), the ML box evolves similarly to the PC box, though it experiences substantial seasonal cycling because of its interaction with

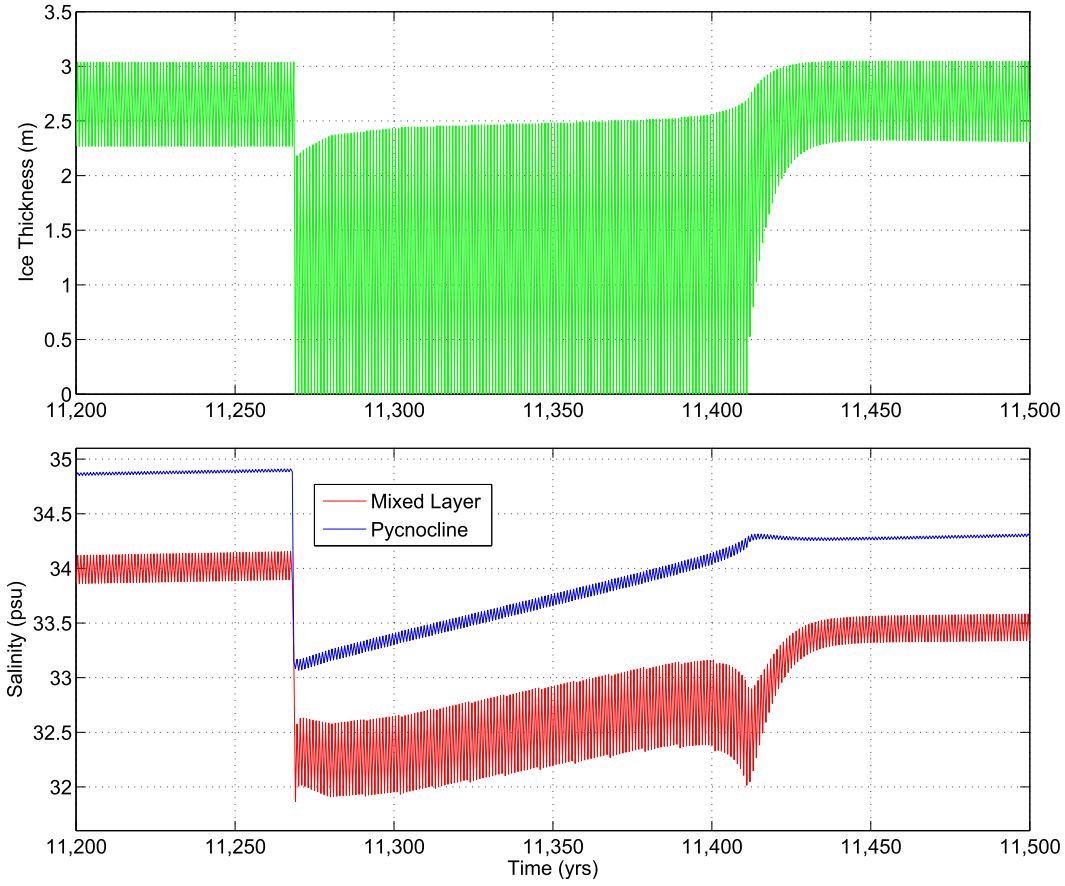

FIG. 4. Unsmoothed model output showing the seasonal evolution of (top) sea ice thickness and (bottom) salinities of the ML and PC ocean boxes during a typical interstadial event. This model output is biannual, with all state variables reported at the end of the winter (cold) season and at the end of the summer (warm) season.

the atmosphere and sea ice (see Figs. 5 and 6). Following this initial rapid decay, we also discern that there is a phase of slow decay (with a long time scale of several hundred years), in which the maximum thickness of the sea ice increases gradually (from 2.2 to 2.5 m; Fig. 4) and the temperatures of the ML and PC boxes decay slowly (from 1.5° to 1.2°C in both the ML and PC boxes; Fig. 6). The salinities of the PC and ML boxes, which briefly equalized at the beginning of the interstadial period because of rapid sea ice melt and eddy-driven vertical exchange, diverge during the interstadial, and the ML and PC layers begin to restratify: as the maximum winter thickness of the sea ice increases throughout this period, this results in a net flux of brine into the PC box, thereby increasing its salinity and density (Figs. 7–9).

The transition back to the stadial phase, in which the system has year-round sea ice cover, is slower than the abrupt transition to the interstadial phase. There appear to be two time scales associated with this transition. There is a short time scale of approximately 10–20 yr associated with the summer temperature of the ML box returning to below −1.0°C, the sea ice thickness returning to its stadial range, and the end-of-winter atmospheric temperature returning to −22°C (Figs. 4 and 6). There is also a longer time scale of approximately 50 yr associated with the time required for the pycnocline temperature and the end-of-summer ice thickness to relax to their averaged stadial values, −1.0°C and 2.3 m, respectively.

Figure 10 provides a pictorial summary of the major processes that characterize the stadial and interstadial phases in the model. The difference between the fluxes in the two phases results from major differences in the sea ice cover: a substantial, perennial sea ice cover during the stadial period and a thinner, seasonal sea ice cover during the interstadial. During the stadial phase, a robust perennial ice cover allows for vigorous ice export and accompanying freshwater recirculation into the DP layer; during the interstadial, both export and recirculation are comparatively weaker as there is less ice to export. During the interstadial phase, the column spends a significant amount of time in an ice-free state,

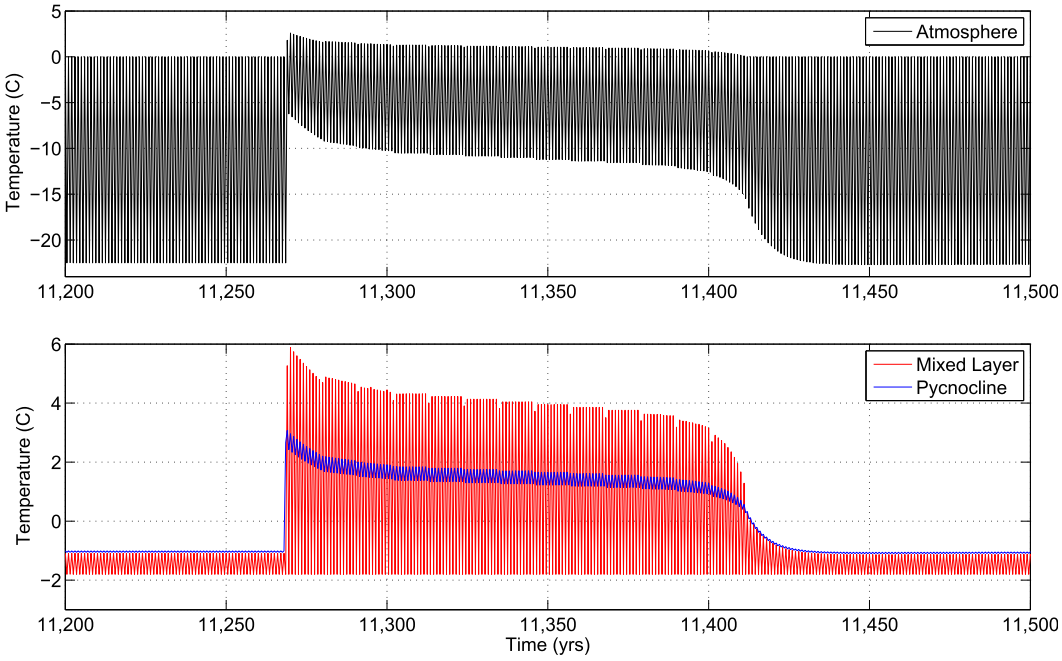

FIG. 5. Results from one typical model interstadial phase, showing (top) surface atmospheric, and (bottom) ML and PC temperatures. This model output is unsmoothed and biannual, with all state variables reported at the end of the winter (cold) season and at the end of the summer (warm) season. Note the strong seasonal cycle in surface and ML temperatures and the relative lack of a seasonal cycle in the PC.

and the resulting wind-driven mixing between the ML and PC boxes is strong compared to that during the stadial phase. The perennial sea ice cover during the stadial is augmented by polynya ice, which is imported into the column (with its accompanying brine), while the interstadial column, which only possesses a seasonal sea ice cover, does not receive extra ice and brine input from polynyas. During the interstadial phase, large amounts of sea ice grow and melt annually with the seasonal cycle, whereas during the stadial phase this seasonal cycle in sea ice cover is much smaller. As a consequence, the input of freshwater into the ML box from melt and the PC box from brine rejection is much larger during the interstadial than the stadial. Finally, as we have summarized in Table 1, the OHFC during the stadial period is into the DP box, while the OHFC during the interstadial is shared by the ML and PC boxes.

4. Sensitivity studies

a. *OHFC parameters*

Figure 11 provides an overview of the sensitivity of the stadial and interstadial time scales to changes in the OHFC parameters, $Q_{\text{tot}}^{\text{NoIce}}$ and $Q_{\text{tot}}^{\text{Ice}}$. First and foremost, we see that for the model to support D-O-like oscillations, the net heat transport into the Nordic seas must be small throughout the cycle, comparable to that seen today in the Arctic, and a small fraction of that into the Nordic seas today. This finding is consistent with our supposition that the sinking branch of the AMOC terminates south of the Nordic seas throughout the glacial period and that the position of this sinking branch is relatively insensitive to the state of the Nordic seas.

In general, we see that the model produces robust oscillations over a reasonable range of values of these OHFC parameters and that this range is between one to two orders of magnitude less than the OHFC into the Nordic seas today. In particular, we see that oscillations reminiscent of D-O events (with interstadial phases greater than 75 yr in length and with total cycles between 1000 and 1500 yr in length) occur over a 50% change in $Q_{\text{tot}}^{\text{NoIce}}$ and a 40% change in $Q_{\text{tot}}^{\text{Ice}}$.

The ranges of $Q_{\text{tot}}^{\text{NoIce}}$ and $Q_{\text{tot}}^{\text{Ice}}$ in Fig. 11 were chosen to highlight the central region about which physically relevant oscillations exist, given the default parameter values listed in Table 2. We note that oscillations still occur for $Q_{\text{tot}}^{\text{Ice}} < 0.4\,\text{W m}^{-2}$ and $Q_{\text{tot}}^{\text{NoIce}} < 0.75\,\text{W m}^{-2}$ (even though the length of the interstadial phase is less than 75 yr), suggesting that the oscillations themselves are robust to changes in OHFC values; the length of the interstadial phase, however, is more sensitive to such changes.

To produce Fig. 11, we have defined the onset of the interstadial phase as when the PC and DP boxes become

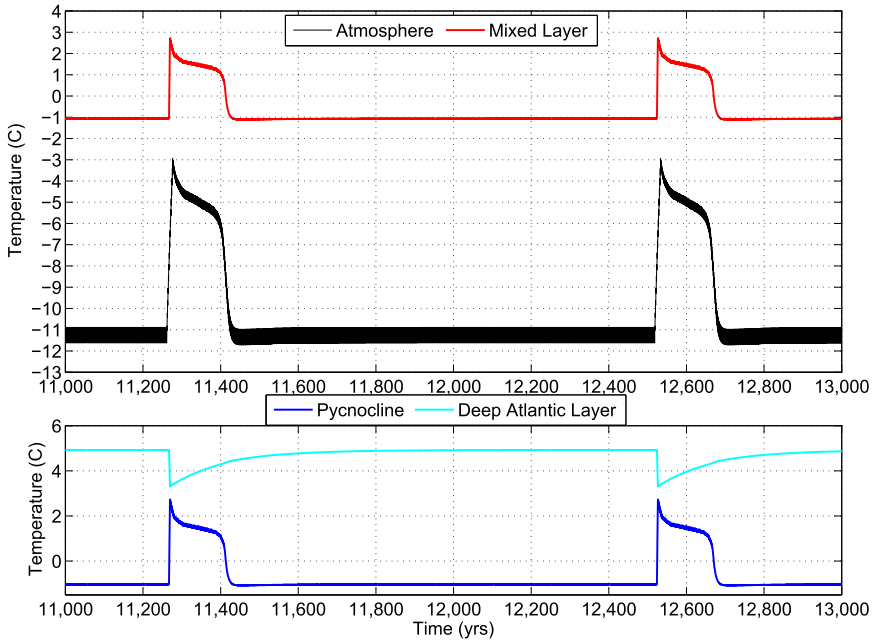

FIG. 6. Results from one model D-O cycle, showing (top) surface temperature and (bottom) ocean box temperatures. Ocean box temperatures have been smoothed with a 2-yr running-mean filter, while the surface temperature has been smoothed with a 25-yr running-mean filter. Note that the 25-yr running-mean filter used on the surface temperature output makes the transition from the stadial (cold) phase to interstadial (warm) phase appear earlier on the surface temperature time series than the others.

buoyantly unstable and overturn (as described in section 3); the end of the interstadial phase (and beginning of the stadial phase) is defined to be when the temperature of the PC box has relaxed to 0.1°C of its stadial value; and the time required for a single cycle (stadial plus interstadial phases) is taken to be the time between overturning events. It is possible for the interstadial phase to go on forever (hatched regions of Fig. 11) when the ML and PC boxes cannot rid themselves of excess heat, a requirement if perennial sea ice is to reform. Whether the model reforms perennial sea ice depends on several bifurcation parameters. We will carefully consider these parameters and their implications in a forthcoming paper.

From examining Fig. 11, we see that the total OHFC when ice is present ($Q_{\text{tot}}^{\text{Ice}}$) affects the length of the stadial, and hence how long it takes for the ocean column to become convectively unstable and overturn. Such a process brings deep ocean heat up to the surface and melts the ice, initiating the interstadial phase. On the other hand, we see that the total OHFC when ice is absent ($Q_{\text{tot}}^{\text{NoIce}}$) affects the interstadial time scale, the time required for the column to cool and support the regrowth of perennial sea ice. We will further describe the relationship of these and other parameters to the lengths of the interstadial and stadial phases in section 4e.

b. *Vertical distribution of OHFC during ice-free conditions*

In our control simulation, we have apportioned $Q_{\text{tot}}^{\text{NoIce}}$, the total (vertically integrated) OHFC during ice-free conditions, as follows: two-thirds of the total heat flux enters the ML box and one-third of the total heat flux enters the PC box. The sensitivity to the choice of how we distribute the OHFC vertically is tested in two alternate model configurations: one with a larger proportion of the ice-free OHFC concentrated in the ML box and less in the PC box and one with a smaller proportion of ice-free OHFC concentrated in the ML box and more in the PC.

Table 3 shows the sensitivity of the model to such changes in the distribution of $Q_{\text{tot}}^{\text{NoIce}}$. Here, we present the time scales produced by the model in the case where we have modified the value of B_T to $5.5\,\text{W}\,\text{m}^{-2}\,^{\circ}\text{C}^{-1}$ (from $5.0\,\text{W}\,\text{m}^{-2}\,^{\circ}\text{C}^{-1}$) and have left the values of other control parameters unchanged. We record the length of the interstadial phase and cycle duration when the ratio of OHFC into the ML and PC boxes are shifted from 2:1 (as in the control) to 1:1 (more of total OHFC into the PC box) and 3:1 (more of total OHFC into the ML box). We find that, while the lengths of the stadial and interstadial phases are modified by this choice, the fundamental

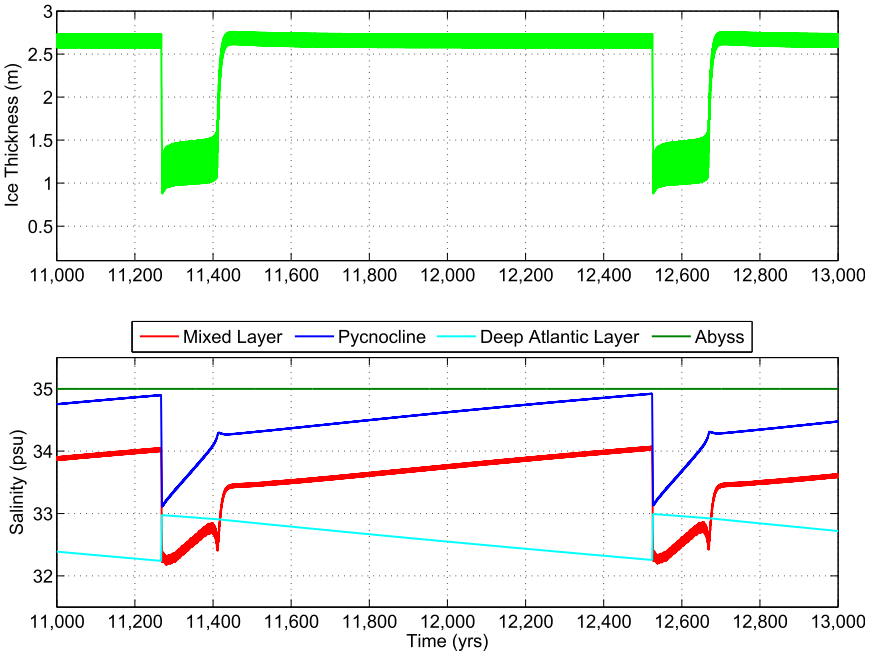

FIG. 7. Results from one model D-O cycle, showing (top) sea ice evolution and (bottom) ocean box salinities. All raw model output, originally reported biannually, has been smoothed with a 5-yr running-mean filter.

behavior of the model (oscillations between stadial and interstadial phases on a millennial time scale) does not change appreciably (the changes in the length of the stadial and interstadial phases in the 3:1 and 1:1 cases are within 5% and 60%, respectively, of those in the 2:1 control case). Therefore, we conclude that the model is robust to changes in the vertical distribution of OHFC during ice-free conditions.

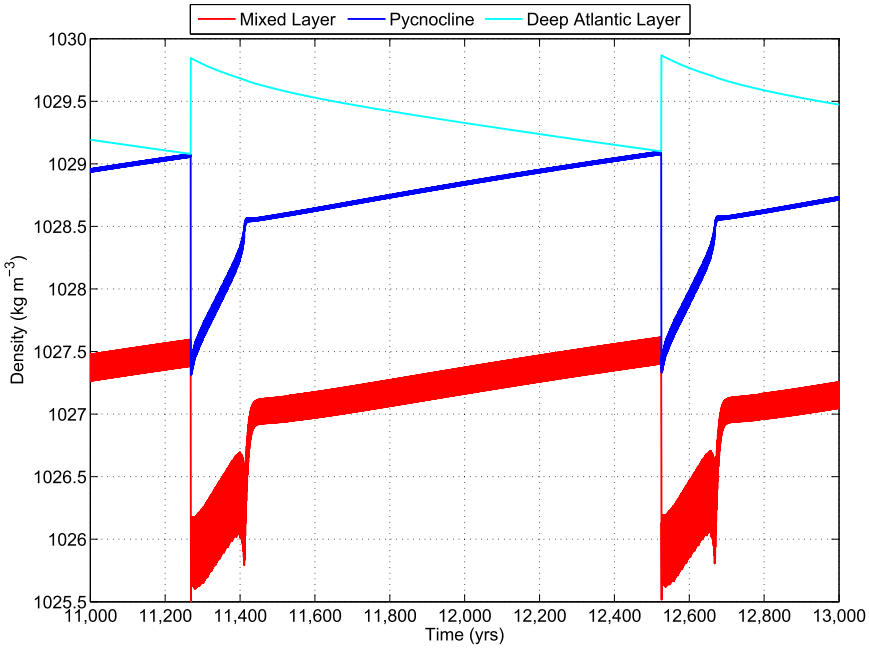

FIG. 8. The 2000 yr of unsmoothed model output showing the evolution of the densities of the ML, PC, and DP boxes.

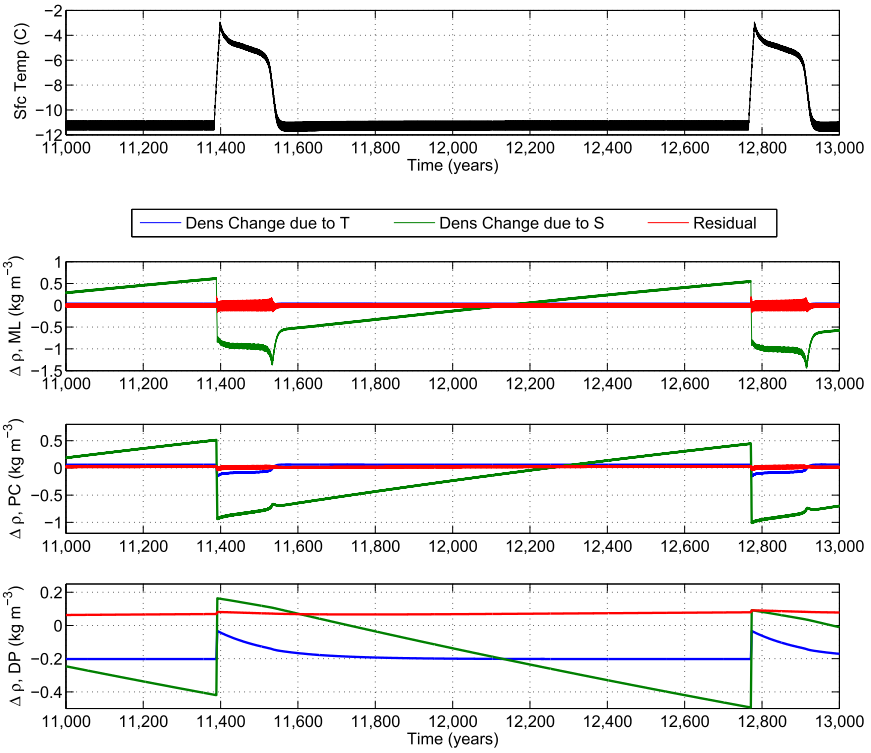

FIG. 9. The 2000 yr of smoothed model output showing (top)–(bottom) surface temperature and the density differences (relative to a reference density) of the ML, PC, and DP boxes over time. For a given layer, the density difference resulting from temperature is $\Delta\rho_T = (\partial\rho/\partial T)_0\Delta T$ and the density difference resulting from salinity is $\Delta\rho_S = (\partial\rho/\partial S)_0\Delta S$, where $(\partial\rho/\partial T)_0$ and $(\partial\rho/\partial S)_0$ are computed at reference temperatures and salinities for each layer and ΔT and ΔS are defined with respect to a reference temperature and salinity for each layer. The residual term is defined as $\Delta\rho_{\rm res} = \rho - \rho_0 - \Delta\rho_T - \Delta\rho_S$. Model output, originally reported biannually, has been smoothed with a 5-yr running-mean filter.

c. *Temporal variability in ocean and atmospheric heat flux convergence*

1) OHFC

Observational studies show that the OHFC into the Nordic seas today is variable on interannual time scales on the order of 5–10 yr (see Hatun et al. 2005). Although the North Atlantic gyre is displaced southward in the glacial climate due to changes in the wind stress curl (see, e.g., Li and Battisti 2008; Braconnot et al. 2007; Laînè et al. 2009), we explore the impact of general stochastic variability in the OHFC on the modeled D-O cycles by adding a red noise component to $Q_{\rm tot}^{\rm NoIce}$,

$$(Q_{\rm tot}^{\rm NoIce})_i = \lambda(Q_{\rm tot}^{\rm NoIce})_0 + (1-\lambda)(Q_{\rm tot}^{\rm NoIce})_{i-1} + \epsilon, \qquad (23)$$

where λ is Δt over the time scale over which OHFC is said to be variable (for $\Delta t = 1$ yr, realistic modern variability in the OHFC is simulated when $\lambda = 1/5$–$1/10$) and ϵ is the appropriately scaled white noise process. Substituting such a process for our static $Q_{\rm tot}^{\rm NoIce}$ with other parameters held at their control values results in an increase in the length of the interstadial phase, from 150 yr to nearly 180 yr. Furthermore, we find the phase space that supports physically relevant oscillations (as defined in section 4a above) is widened in the $Q_{\rm tot}^{\rm NoIce}$ dimension by approximately 10% with such a modification (not shown). Thus, simulating the interstadial heat flux convergence as a red noise process tends to increase the robustness of the model.

2) ATMOSPHERIC HEAT FLUX CONVERGENCE

It is known that the atmospheric heat transport into the polar regions is also variable (see Overland and Turet 1994). This variability is well approximated as white noise and may be added to D as a good representation of this real physical phenomenon. When white noise with a standard deviation of 5 W m^{-2} is added to D with all model parameters maintained as in Table 2 (the "default" parameter regime), the average length of the interstadials increases from 180 to 210 yr (with

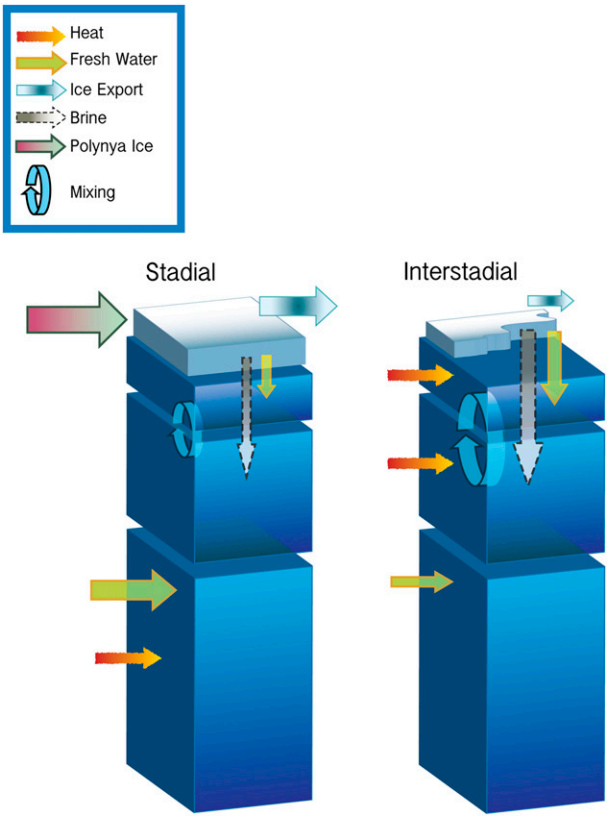

FIG. 10. Schematic figure depicting the key processes characterizing the stadial and interstadial periods, which all result from differences in the sea ice cover in the two states. During the interstadial period, the substantial seasonal cycle of sea ice results in large freshwater and brine fluxes into the ML and PC. Furthermore, the seasonal ice cover of the interstadial fosters more wind-driven mixing between the ML and PC boxes, less ice export and accompanying freshwater recirculation, and OHFC into the surface layers. In contrast, the muted seasonal cycle of sea ice during the stadial phase results in smaller melt and brine rejection fluxes. The thicker, year-round sea ice cover of the stadial, which is augmented by polynya ice import, inhibits wind-driven mixing between the ML and PC boxes, enhances ice export and accompanying freshwater circulation, and diverts OHFC from the surface layers into the DP box.

a standard deviation of 100 yr), while the average length of a cycle remains approximately unchanged.

d. Polynya activity

Removing the polynya parameterization in the model [setting $\int_{1\text{yr}}(dp_{\text{ice}}/dt)\,dt = 0$], while leaving all other parameters at their default values prevents cycling between stadial and interstadial states. Rather than oscillating, the model remains in an interstadial state perpetually. Retuning other model parameters does not prevent this. Thus, one robust result from our model is that ice production in latent heat polynyas are a prerequisite for D-O cycles: removing this term precludes the system from oscillating between stadial and interstadial states.

e. General sensitivity to parameter choices

Table 4 displays the general sensitivity of the model to key parameter values. From examining the table, we see that the parameters broadly fall into two categories: those that tend to change the length of the stadial phase and those that tend to change the length of the interstadial phase. In a subsequent paper, we will provide a detailed analysis of how changes in these parameters affect the lengths of the stadial and interstadial phases and the time scales therein. Here, we provide a brief overview of these parameter dependencies, and attempt to obtain an intuitive sense of how the behavior of the model is affected by these different classes of parameters.

The parameters that change the length of the stadial phase are those that affect the rate the column becomes buoyantly unstable and overturns. Overturning is initiated by buoyant instability between the PC and DP boxes (see section 3). Thus, parameters that affect ρ_{PC} and ρ_{DP}, the densities of the pycnocline and deep layers, will tend to affect the length of the stadial phase of the oscillation; these include C_r, the ice export factor, and $Q_{\text{tot}}^{\text{Ice}}$, the OHFC. If C_r is increased, the salinity of the PC box increases and the salinity of the DP box decreases at a faster pace, shortening the time it takes for ρ_{PC} to equal ρ_{DP} and shortening the stadial phase. Similarly, if $Q_{\text{tot}}^{\text{Ice}}$ is increased, the temperature of the DP box increases at a faster pace, again shortening the time required for ρ_{PC} to equal ρ_{DP} and thus shortening the length of the stadial phase.

The length of the interstadial phase is determined by the longest interstadial time scale, which depends on a combination of parameters related to the delivery of heat into the mixed layer. During the interstadial phase, there is a delicate balance between the rate at which heat is delivered into the mixed layer and the rate at which it is fluxed from the mixed layer to the atmosphere; shifting this balance toward the former lengthens the interstadial, while shifting it toward the latter tends to shorten it. In general, $Q_{\text{tot}}^{\text{NoIce}}$ (the OHFC during ice-free conditions) and $K_{\text{ML-PC}}^{\text{NoIce}}$ (the mixing coefficient between the ML and PC boxes during ice-free conditions) are both related to the rate at which heat is delivered into the ML, while B_T is related to the rate at which heat is fluxed out of the ML. Increasing $Q_{\text{tot}}^{\text{NoIce}}$ and $K_{\text{ML-PC}}^{\text{NoIce}}$ tends to lengthen the interstadial time scale up to a certain point beyond which further increases in these parameters prevent the system from returning to a stadial phase. Similarly, decreasing B_T tends to lengthen the interstadial phase up to a certain point, when any further

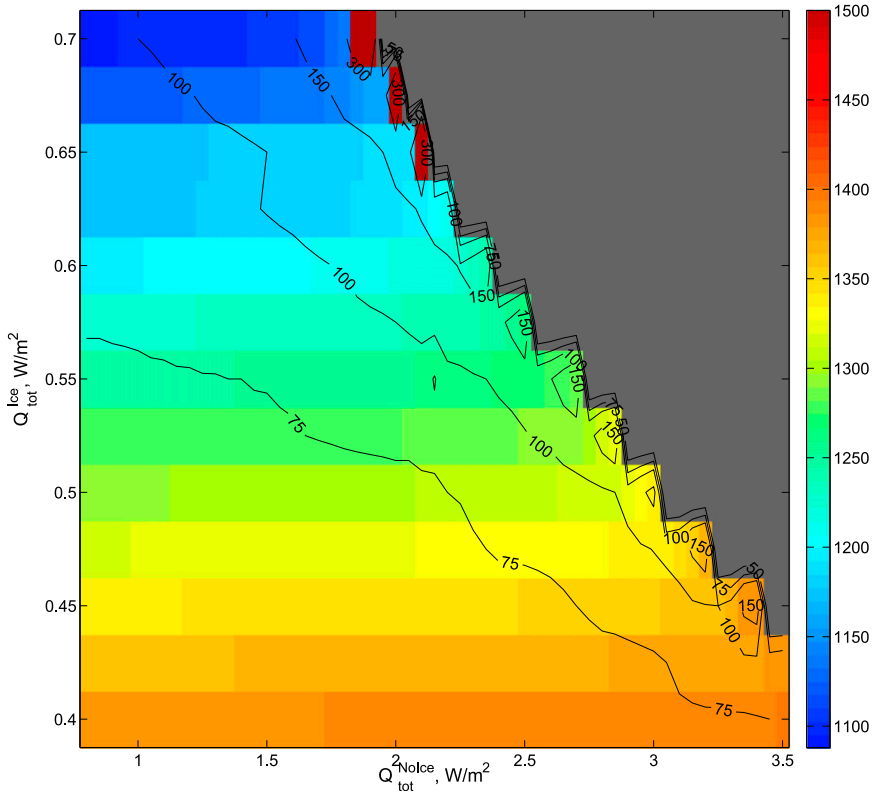

FIG. 11. Model sensitivity to OHFC parameters $Q^{\mathrm{NoIce}}_{\mathrm{tot}}$ (ice free) and $Q^{\mathrm{Ice}}_{\mathrm{tot}}$ (ice covered). The contours represent the average length of the interstadial phase (in years), while the color shades represent the average length of the entire cycle (in years). Areas that do not support D-O-type oscillations have been shaded in gray.

decreases tend to prevent the system from returning to the stadial.

5. Discussion and implications

a. Discussion

As with any idealized model, the purpose of our model is to illuminate the essential ingredients responsible for the gross characteristics of D-O cycles, particularly the time scales of the stadial and interstadial phases, the abrupt transition from stadial to interstadial phase, and the gentler transition back from the interstadial to the stadial phase. Our results show that a model of the area-averaged conditions in the Nordic seas that combines an energy-balance atmosphere, a one-layer sea ice model (which includes parameterizations of polynyas, ice export, and fractional ice cover), and four stacked ocean boxes (representing the gross hydrographic structure of the Nordic seas) can exhibit the gross characteristics of the D-O cycles, including the observed hydrographic structure (Rasmussen and Thomsen 2004; Dokken et al. 2013), the time scales associated with the stadial and interstadial phases, and the time scales associated with the transitions between phases.

Proxy data from the GRIP and GISP ice cores show that the D-O oscillations occur with a periodicity of approximately 1500 yr, with the length of the interstadial phase persisting anywhere between 100 and 1000 yr and the stadial phase occupying the remainder of the period (Rahmstorf 2002). Our model compares reasonably with these observations: within the explored parameter space where physically relevant oscillations exist, the total length of a modeled D-O cycle is anywhere from 1000 to 1500 yr and the length of the interstadial phase is anywhere from 75 to 500 yr. While the total length of the modeled cycle and the length of the stadial phase agree well with observational data, the length of the modeled interstadial phase is significantly shorter than that seen in the proxy record.

According to the ice core record, the transitions from the stadial to interstadial phase appear to be nearly instantaneous in the Greenland record, suggesting a time scale of less than 20 yr for this transition (i.e., the temporal resolution of the Greenland ice cores record). Our model results show transitions from the stadial to the interstadial

TABLE 2. Values of constants and default parameter values used to generate model results.

Depth of ocean boxes (m)	
Depth of ML h_{ML}	50
Depth of PC h_{PC}	300
Depth of DP h_{DP}	800
Depth of AB h_{AB}	3000
Mixing coefficients ($m^2\,s^{-1}$)	
K^{T-Ice}_{ML-PC}	1.0×10^{-4}
K^{S-Ice}_{ML-PC}	1.0×10^{-4}
$K^{T-NoIce}_{ML-PC}$	6.0×10^{-4}
$K^{S-NoIce}_{ML-PC}$	6.0×10^{-4}
K^{T}_{PC-DP}	1.0×10^{-5}
K^{S}_{PC-DP}	1.0×10^{-6}
K^{T}_{DP-AB}	1.0×10^{-7}
K^{S}_{DP-AB}	1.0×10^{-8}
Optical depths	
n_s, ice covered	2.8
n_s, ice free	2.9
n_w, ice covered	2.5
n_w, ice free	2.5
Other ice and ML parameters	
α_{ice}	0.65
α_{ocn}	0.1
Ice–ocean conductive flux constant C_0 ($W\,m^{-2}\,°C^{-1}$)	20
Atmospheric heat transport D ($W\,m^{-2}$)	90
OLR constant A ($W\,m^{-2}$)	320
Temperature-dependent OLR constant B ($W\,m^{-2}\,°C^{-1}$)	4.6
Summer shortwave radiation F_{SW} ($W\,m^{-2}$)	200
ML turbulent heat flux parameter B_T ($W\,m^{-2}\,°C^{-1}$)	5.0
Thermal conductivity of sea ice k ($W\,m^{-1}\,°C^{-1}$)	2.0
Brine and polynya parameters	
Range of h_{ice} in which polynyas add ice to the column (m)	[1.0, ∞)
Ice added by polynyas each year $h^{polynas}_{ice}$ (m)	1.0
Sea ice export residual brine C_r	0.05
Fraction of freshwater recirculation flux into PC F_{PC}	0.80
OHFC parameters ($W\,m^{-2}$)	
Ice-free OHFC Q^{NoIce}_{tot}	3.0
Ice-covered OHFC Q^{Ice}_{tot}	0.5

TABLE 3. Sensitivity of the model to changes in the relative distribution of the ocean heat flux distribution in the mixed layer and pycnocline boxes during ice-free conditions. All parameters are as in the control case but with $B_T = 5.5\,W\,m^{-2}\,°C^{-1}$.

Heat flux convergence distribution, $Q^{trans}_{ML,NoIce}$: $Q^{trans}_{PC,NoIce}$	Interstadial length, cycle duration
1:1	180, 1170
2:1	110, 1210
3:1	85, 1245

phase occur in less than 5 yr, consistent with the observations. In contrast, the transition from the interstadial to the stadial phase in the ice core records appears to take over 100 yr and possibly longer. Our model results, however, show this transition occurs within 20–40 yr, which represents a significant disagreement with observations.

In summary, we find that there are two major discrepancies between our modeled oscillations and those seen in the proxy record: in our model the length of interstadial phase is too short compared to observations and the length of the transition from the interstadial to stadial phase is too abrupt. These differences may be a result of missing physics in our model, or they may be a result of the coarse layering of the ocean column, the lack of horizontal resolution within the Nordic seas, or the absence of stochastic processes. We have gauged the sensitivity of our model to stochastic variations in the OHFC and atmospheric heat transport (see section 4a) and found that adding this variability increased the length of the interstadial phase, though not enough to account for the discrepancy from observations. We believe that future work on this hypothesis could focus on accurate modeling of horizontal transport and mixing processes within the Nordic seas as well as on increasing the vertical resolution of the ocean column.

We also note that our model results are consistent with observational inferences (see section 1a) that indicate a stadial increase in deep temperature of 2°C prior to overturning (Rasmussen and Thomsen 2004; Dokken et al. 2013). Additionally, our results corroborate other observational inferences suggesting rigorous sea ice production and accompanying brine rejection along the FSIS is essential for D-O cycles (Dokken et al. 2013).

The model results of Winton and Sarachik (1993), Loving and Vallis (2005), and de Verdière and Raa (2010) feature oscillations in the AMOC that are reminiscent of the observed D-O cycles. By contrast, our

TABLE 4. General sensitivity of the model time scales (length of stadial phase and length of interstadial phase) to changes in model parameters.

Parameter change	Effect on stadial	Effect on interstadial
Increase B_T	Little effect	Shorten
Increase C_r	Shorten	Little effect
Increase Q^{Ice}_{tot}	Shorten	Little effect
Increase Q^{NoIce}_{tot}	Little effect	Lengthen
Increase dp_{ice}/d_t	More ice	Shorten
Increase ice threshold for polynyas	Little effect	Lengthen
Increase K^{NoIce}_{ML-PC}	Little effect	Lengthen

model features D-O cycles resulting from interactions within an atmosphere–sea ice–ocean column, rather than within an Atlantic Ocean scale model: changes in the ocean stratification and sea ice cover within the Nordic seas that are the hallmark of our model D-O cycles are independent of any changes in the heat and salt transport associated with the AMOC. In fact, our model suggests that D-O cycles will only exist if the sinking branch of the AMOC does not extend into the Nordic seas (as it does in the present climate): the system will only support a stadial state when ocean heat transport into the Nordic seas is less than 0.005 PW ($3\,W\,m^{-2}$ averaged over the area of the Nordic seas), which is a small fraction of what is delivered into the Nordic seas today.

In general, we hypothesize that ocean heat transport incident on an ice-covered region will tend to subduct and circulate under a cold halocline, while ocean heat transport incident on a region that is ice free will tend to concentrate in the upper ocean and converge there while it fluxes into the atmosphere. In the former case, very little heat will converge into the region, while in the latter case, a slightly larger amount of heat will converge. Hence, the sea ice cover causes changes in the distribution of OHFC that feed back on the sea ice cover itself. Work by Bitz et al. (2006) used GCM results to argue that transitioning from perennial to seasonal sea ice in the Arctic enhanced brine rejection along the Siberian shelf, resulting in an increase in the OHFC into the region. Such changes occurred despite a weakening in the strength of the AMOC south of the subpolar seas (Bitz et al. 2006). Thus, the OHFC changes we prescribe account for differences in the vertical distribution of how heat converges locally in the presence or absence of sea ice and a cold halocline and are independent of the AMOC.

Consistent with the small value of OHFC, the only advective salt flux convergence (ASFC) in our model is into the DP box, and it is used to balance the freshwater flux out of the Nordic seas associated with sea ice export. Physically, we envision that exported sea ice melts in the North Atlantic, entrains into the sinking branch of the AMOC, and returns at depth to the Nordic seas. The lack of ASFC into the top two boxes is supported by GCM simulations run with Last Glacial Maximum (LGM) boundary conditions, which show that the ASFC into the Nordic seas is very small [see Braconnot et al. 2007; see also the Paleoclimate Modelling Intercomparison Project 2 (PMIP2) archive].

In our model, the slight difference in the magnitudes of the ice-covered and ice-free OHFC only affects the details of the modeled oscillations, not the oscillations themselves or the hydrographic structures of the stadial and interstadial phases. Imposing an ice-covered and ice-free OHFC that are both equal to $1\,W\,m^{-2}$, for example, results in modeled D-O oscillations with an interstadial phase of 150 yr and a full cycle period of 850 yr.

Modeling results (Brandefelt and Otto-Bliesner 2009) support our assumption that the Nordic seas were relatively disconnected from the AMOC throughout the last glacial period. In the modern climate, the wind-driven subpolar gyre efficiently delivers heat and salt into the Nordic seas; as a result, the sinking branch of the AMOC resides in the Nordic seas. In the glacial climate, however, GCM simulations suggest that the Laurentide ice sheet deflected the atmospheric jet southward and reduced the storminess over the North Atlantic (Braconnot et al. 2007; Laînè et al. 2009). Consistent with the southward deflection of the jet, long-equilibration coupled climate model simulations (Brandefelt and Otto-Bliesner 2009) suggest the AMOC was weaker and shallower during the glacial period and the sinking branch was shifted southward from today's position in the Nordic seas.

b. *Implications*

Our model helps explain why D-O cycles are not present in the Holocene. As discussed in section 4e, D-O cycles are only possible when the ocean heat imported to the Nordic seas is small, less than 0.005 PW ($3\,W\,m^{-2}$ multiplied by the area of the Nordic seas). The OHFC into the Nordic seas today is about 0.05 PW (Hansen and Osterhus 2000), which is an order of magnitude higher.

Further reasons why the Nordic seas do not experience stadial conditions and D-O-type oscillations during the Holocene may also include the current position of the midlatitude storm track and the lack of substantial polynya activity, both of which make it difficult to form a strong halocline in the region today. Today, the midlatitude storm track traverses the Nordic seas; during glacial times, on the other hand, proxy evidence (see Pailler and Bard 2002) and modeling results (see, e.g., Li and Battisti 2008; Braconnot et al. 2007; Laînè et al. 2009) suggest that the midlatitude storm track was shifted equatorward from its current position. While conditions within the Nordic seas during the last glacial period may have been quiescent enough to support the formation of a strong halocline, the current position of the storm track may preclude the existence of a halocline because of significant wind-driven mixing of the upper ocean in the region. Without a halocline, sea ice formed in the region (if any) would be unable to persist because of heat fluxes from warmer waters below. In the Arctic basin today, the presence of a strong halocline is crucial for preventing warmer circulating Atlantic waters below from melting the sea ice (Aagaard et al.

1981). In addition to the current position of the storm track, the lack of polynya activity in the Holocene would also make it more difficult to form a strong halocline.

The proxy record of the last glacial period presents another interesting conundrum regarding millennial-scale variability: D-O oscillations, which were robust and plentiful during the glacial period prior to 24 kyr before present, were absent during the LGM itself. The results of our model suggest that latent heat polynyas, which formed off the edge of the Fennoscandian ice sheet (FSIS) during the last glacial period, were essential for the D-O oscillations: polynyas are required for returning the Nordic seas to the stadial phase of the D-O cycle and for maintaining the stratification between the ML and PC throughout the stadial phase. During the LGM, the FSIS was believed to extend to the continental shelf. While katabatic winds would have still emanated from the FSIS in this case and latent heat polynyas would still result, conditions would have been much colder with more brine rejected. The continental slope bathymetry over which the brine rejected from such polynyas would traverse would be much different from the extensive continental shelf over which it flowed and entrained during the glacial. In the former case, it is possible that the resulting large volume of cold brine flowing down the continental slope could not entrain enough ambient water to interleave into the halocline. Consequently, the brine would sink to the bottom of the water column, in a manner analogous to deep-water formation in coastal polynyas in the present-day Weddell Sea. Thus, it is possible that the region only supported a weak halocline, and incoming heat from the North Atlantic converged into the deep would not be trapped and decoupled from the surface (as we hypothesize is characteristic of the stadial phases of the D-O cycles) but rather gradually vented, reducing the thickness of the sea ice in the Nordic seas. In such a case, there would be insufficient buildup of deep ocean heat and pycnocline salt to initiate a convective overturning event, and the Nordic seas would remain in a perpetual stadial phase.

Acknowledgments. We wish to acknowledge grants from the Comer Foundation and the U.S. Department of Energy Computational Science Graduate Fellowship (DOE CSGF); Aaron Barker for composing Fig. 10; and the helpful comments, suggestions, and critiques of three anonymous reviewers, whose thoughtful input improved the quality of the work substantially.

REFERENCES

Aagaard, K., L. K. Coachman, and E. Carmack, 1981: On the halocline of the Arctic Ocean. *Deep-Sea Res.,* **28A,** 529–545, doi:10.1016/0198-0149(81)90115-1.

Alley, R., 2007: Wally was right: Predictive ability of the North Atlantic conveyer belt hypothesis for abrupt climate change. *Annu. Rev. Earth Planet. Sci.,* **35,** 241–272, doi:10.1146/annurev.earth.35.081006.131524.

Bitz, C. M., P. R. Gent, R. A. Woodgate, M. M. Holland, and R. Lindsay, 2006: The influence of sea ice on ocean heat uptake in response to increasing CO_2. *J. Climate,* **19,** 2437–2450, doi:10.1175/JCLI3756.1.

——, J. C. H. Chiang, W. Cheng, and J. J. Barsugli, 2007: Rates of thermohaline recovery from freshwater pulses in modern, Last Glacial Maximum and greenhouse warming climates. *Geophys. Res. Lett.,* **34,** L07708, doi:10.1029/2006GL029237.

Bond, G. C., and R. Lotti, 1995: Iceberg discharges into the North Atlantic on millennial time scales during the last glaciation. *Science,* **267,** 1005–1010, doi:10.1126/science.267.5200.1005.

Braconnot, P., and Coauthors, 2007: Results of PMIP2 coupled simulations of Mid-Holocene and Last Glacial Maximum—Part 1: Experiments and large-scale features. *Climate Past,* **3,** 261–277, doi:10.5194/cp-3-261-2007.

Brandefelt, J., and B. Otto-Bliesner, 2009: Equilibration and variability in a Last Glacial Maximum climate simulation with CCSM3. *Geophys. Res. Lett.,* **36,** L19712, doi:10.1029/2009GL040364.

Cavalieri, D., and S. Martin, 1994: The contribution of Alaskan, Siberian, and Canadian coastal polynyas to the cold halocline layer of the Arctic Ocean. *J. Geophys. Res.,* **99** (C9), 18 343–18 362, doi:10.1029/94JC01169.

Chiang, J. C. H., and C. M. Bitz, 2005: Influence of high latitude ice cover on the marine intertropical convergence zone. *Climate Dyn.,* **25,** 477–496, doi:10.1007/s00382-005-0040-5.

——, M. Biasutti, and D. S. Battisti, 2003: Sensitivity of the Atlantic intertropical convergence zone to Last Glacial Maximum boundary conditions. *Paleoceanography,* **18,** 1094, doi:10.1029/2003PA000916.

Clement, A., and L. Peterson, 2008: Mechanisms of abrupt climate change of the last glacial period. *Rev. Geophys.,* **46,** RG4002, doi:10.1029/2006RG000204.

Dansgaard, W., S. Johnsen, H. Clausen, D. Dahl-Jensen, N. Gundestrup, C. Hammer, and H. Oeschger, 1984: North Atlantic climatic oscillations revealed by deep Greenland ice cores. *Climate Processes and Climate Sensitivity, Geophys. Monogr.,* Vol. 29, Amer. Geophys. Union, 288–298.

——, and Coauthors, 1993: Evidence of general instability of past climate from a 250-kyr ice core record. *Nature,* **364,** 218–220, doi:10.1038/364218a0.

de Verdière, A., and L. Raa, 2010: Weak oceanic heat transport as a cause of the instability of glacial climates. *Climate Dyn.,* **35,** 1237–1256, doi:10.1007/s00382-009-0675-8.

Dokken, T. M., and E. Jansen, 1999: Rapid changes in the mode of deep and intermediate water formation linked with atmospheric and ice sheet variations during the last glacial. *Nature,* **401,** 458–461, doi:10.1038/46753.

——, K. H. Nisancioglu, C. Li, D. S. Battisti, and C. Kissel, 2013: Dansgaard-Oeschger cycles: Interactions between ocean and sea ice intrinsic to the Nordic seas. *Paleoceanography,* **28,** 491–502, doi:10.1002/palo.20042.

Duffy, P. B., M. Eby, and A. J. Weaver, 1999: Effects of sinking of salt rejected during formation of sea ice on results of an ocean-atmosphere-sea ice climate model. *Geophys. Res. Lett.,* **26,** 1739–1742, doi:10.1029/1999GL900286.

Elliot, M., L. Labeyrie, T. Dokken, and S. Manthé, 2001: Coherent patterns of ice rafted debris deposits in the Nordic regions

during the last glacial (10–60 ka). *Earth Planet. Sci. Lett.,* **194,** 151–163, doi:10.1016/S0012-821X(01)00561-1.

——, ——, and J.-C. Duplessy, 2002: Changes in North Atlantic deep-water formation associated with the Dansgaard–Oeschger temperature oscillations (60–10 ka). *Quat. Sci. Rev.,* **21,** 1153–1165, doi:10.1016/S0277-3791(01)00137-8.

Ganopolski, A., and S. Rahmstorf, 2001: Rapid changes of glacial climate simulated in a coupled climate model. *Nature,* **409,** 153–158, doi:10.1038/35051500.

Gargett, A., 1984: Vertical eddy diffusivity in the ocean interior. *J. Mar. Res.,* **42,** 359–393, doi:10.1357/002224084788502756.

Gill, A. E., 1982: *Atmosphere-Ocean Dynamics*. Academic Press, 662 pp.

Hansen, B., and S. Osterhus, 2000: North Atlantic-Nordic seas exchanges. *Prog. Oceanogr.,* **45,** 109–208, doi:10.1016/S0079-6611(99)00052-X.

Hatun, H., A. Sando, H. Drange, B. Hansen, and H. Valdimarsson, 2005: Influence of the Atlantic subpolar gyre on the thermohaline circulation. *Science,* **309,** 1841–1844, doi:10.1126/science.1114777.

Huppert, H., and J. Turner, 1981: Double-diffusive convection. *J. Fluid Mech.,* **106,** 299–329, doi:10.1017/S0022112081001614.

Keigwin, L., and E. Boyle, 1999: Surface and deep ocean variability in the northern Sargasso Sea during marine isotope stage 3. *Paleoceanography,* **14,** 164–170, doi:10.1029/1998PA900026.

Kraus, E., and J. Turner, 1967: A one-dimensional model of the seasonal thermocline II. The general theory and its consequences. *Tellus,* **19,** 98–106, doi:10.1111/j.2153-3490.1967.tb01462.x.

Laîné, A., and Coauthors, 2009: Northern Hemisphere storm tracks during the last glacial maximum in the PMIP2 ocean-atmosphere coupled models: Energetic study, seasonal cycle, precipitation. *Climate Dyn.,* **32,** 593–614, doi:10.1007/s00382-008-0391-9.

Li, C., and D. Battisti, 2008: Reduced Atlantic storminess during the Last Glacial Maximum: Evidence from a coupled climate model. *J. Climate,* **21,** 3561–3579, doi:10.1175/2007JCLI2166.1.

——, ——, D. Schrag, and E. Tziperman, 2005: Abrupt climate shifts in Greenland due to displacements in the sea ice edge. *Geophys. Res. Lett.,* **32,** L19702, doi:10.1029/2005GL023492.

Loving, J. L., and G. K. Vallis, 2005: Mechanism for climate variability during glacial and interglacial periods. *Paleoceanography,* **20,** PA4024, doi:10.1029/2004PA001113.

MacAyeal, D., 1993: Binge/purge oscillations of the Laurentide ice sheet as a cause of the North Atlantic's Heinrich events. *Paleoceanography,* **8,** 775–784, doi:10.1029/93PA02200.

Martin, S., R. Drucker, and K. Yamashita, 1998: The production of ice and dense shelf water in the Okhotsk Sea polynyas. *J. Geophys. Res.,* **103** (C12), 27 771–27 782, doi:10.1029/98JC02242.

Nguyen, A., D. Menemenlis, and R. Kwok, 2009: Improved modeling of the Arctic halocline with a subgrid-scale brine rejection parameterization. *J. Geophys. Res.,* **114,** C11014, doi:10.1029/2008JC005121.

Okumura, Y., C. Deser, A. Hu, A. Timmermann, and S. Xie, 2009: North Pacific climate response to freshwater forcing in the subarctic North Atlantic: Oceanic and atmospheric pathways. *J. Climate,* **22,** 1424–1445, doi:10.1175/2008JCLI2511.1.

Otto-Bliesner, B., and E. Brady, 2010: The sensitivity of the climate response to the magnitude and location of freshwater forcing: Last Glacial Maximum experiments. *Quat. Sci. Rev.,* **29,** 56–73, doi:10.1016/j.quascirev.2009.07.004.

Overland, J., and P. Turet, 1994: Variability of the atmospheric energy flux across 70°N computed from the GFDL data set. *The Polar Oceans and Their Role in Shaping the Global Environment, Geophys. Monogr.,* Vol. 85, Amer. Geophys. Union, 313–325.

Pailler, D., and E. Bard, 2002: High frequency palaeoceanographic changes during the past 140,000 year recorded by the organic matter in sediments of the Iberian Margin. *Palaeogeogr. Palaeoclimatol. Palaeoecol.,* **181,** 431–452, doi:10.1016/S0031-0182(01)00444-8.

Pausata, F., D. Battisti, K. Nisancioglu, and C. Bitz, 2011: Chinese stalagmites: Proxies for the Indian monsoon response to an archetypal Heinrich event. *Nat. Geosci.,* **4,** 474–480, doi:10.1038/ngeo1169.

Peixoto, J. P., and A. H. Oort, 1992: *Physics of Climate*. American Institute of Physics, 520 pp.

Rahmstorf, S., 2002: Ocean circulation and climate during the past 120,000 years. *Nature,* **419,** 207–214, doi:10.1038/nature01090.

Rasmussen, T., and E. Thomsen, 2004: The role of the North Atlantic drift in the millennial timescale glacial climate fluctuations. *Palaeogeogr. Palaeoclimatol. Palaeoecol.,* **210,** 101–116, doi:10.1016/j.palaeo.2004.04.005.

Schmittner, A., and T. Stocker, 2001: A seasonally forced ocean–atmosphere model for paleoclimate studies. *J. Climate,* **14,** 1055–1068, doi:10.1175/1520-0442(2001)014<1055:ASFOAM>2.0.CO;2.

Semtner, A., 1976: A model for the thermodynamic growth of sea ice in numerical investigations of climate. *J. Phys. Oceanogr.,* **6,** 379–389, doi:10.1175/1520-0485(1976)006<0379:AMFTTG>2.0.CO;2.

Stouffer, R. J., and Coauthors, 2006: Investigating the causes of the response of the thermohaline circulation to past and future climate changes. *J. Climate,* **19,** 1365–1387, doi:10.1175/JCLI3689.1.

Swingedouw, D., J. Mignot, P. Braconnot, E. Mosquet, M. Kageyama, and R. Alkama, 2009: Impact of freshwater release in the North Atlantic under different climate conditions in an OAGCM. *J. Climate,* **22,** 6377–6403, doi:10.1175/2009JCLI3028.1.

Thorndike, A., 1992: A toy model linking atmospheric thermal radiation to sea ice growth. *J. Geophys. Res.,* **97** (C6), 9401–9410, doi:10.1029/92JC00695.

Vellinga, M., and R. Wood, 2002: Global climatic impacts of a collapse of the Atlantic thermohaline circulation. *Climatic Change,* **54,** 251–267, doi:10.1023/A:1016168827653.

Weaver, A., E. Sarachik, and J. Marotze, 1991: Freshwater flux forcing of decadal and interdecadal ocean variability. *Nature,* **353,** 836–838, doi:10.1038/353836a0.

Welander, P., 1977: Thermal oscillations in a fluid heated from below and cooled to freezing from above. *Dyn. Atmos. Oceans,* **1,** 215–223, doi:10.1016/0377-0265(77)90007-0.

——, 1982: A simple heat-salt oscillator. *Dyn. Atmos. Oceans,* **6,** 233–242, doi:10.1016/0377-0265(82)90030-6.

——, and J. Bauer, 1977: On a differentially heated saltwater-ice system. *Tellus,* **29,** 462–469, doi:10.1111/j.2153-3490.1977.tb00757.x.

Winton, M., and E. Sarachik, 1993: Thermohaline oscillations induced by strong steady salinity forcing of ocean general circulation models. *J. Phys. Oceanogr.,* **23,** 1389–1410, doi:10.1175/1520-0485(1993)023<1389:TOIBSS>2.0.CO;2.

Wunsch, C., and R. Ferrari, 2004: Vertical mixing, energy, and the general circulation of the oceans. *Annu. Rev. Fluid Mech.,* **36,** 281–314, doi:10.1146/annurev.fluid.36.050802.122121.